

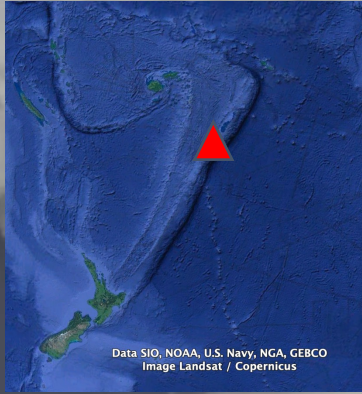
Mechanism of tsunami observed in (near field) and far field

Yuichiro Tanioka, Ayumu Mizutani, Hokkaido University, Japan
Aditya Gusman, GNS New Zealand



Introduction

The 2022 HTHH tsunami

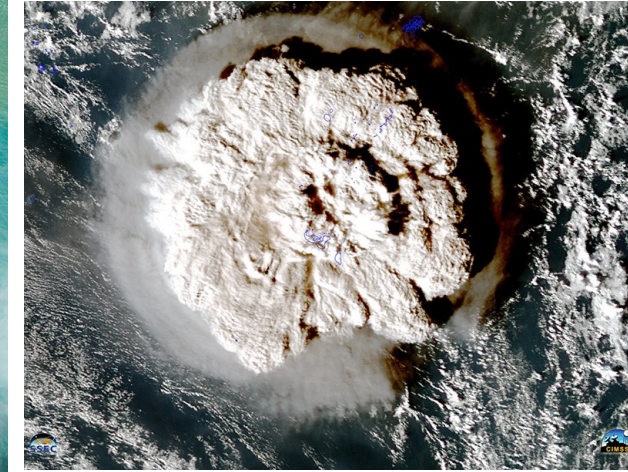


After the 14 January 2022 eruption



HIMAWARI-8

15 January 2022 eruption



After the 15 January 2022 eruption



Tsunami Inundation

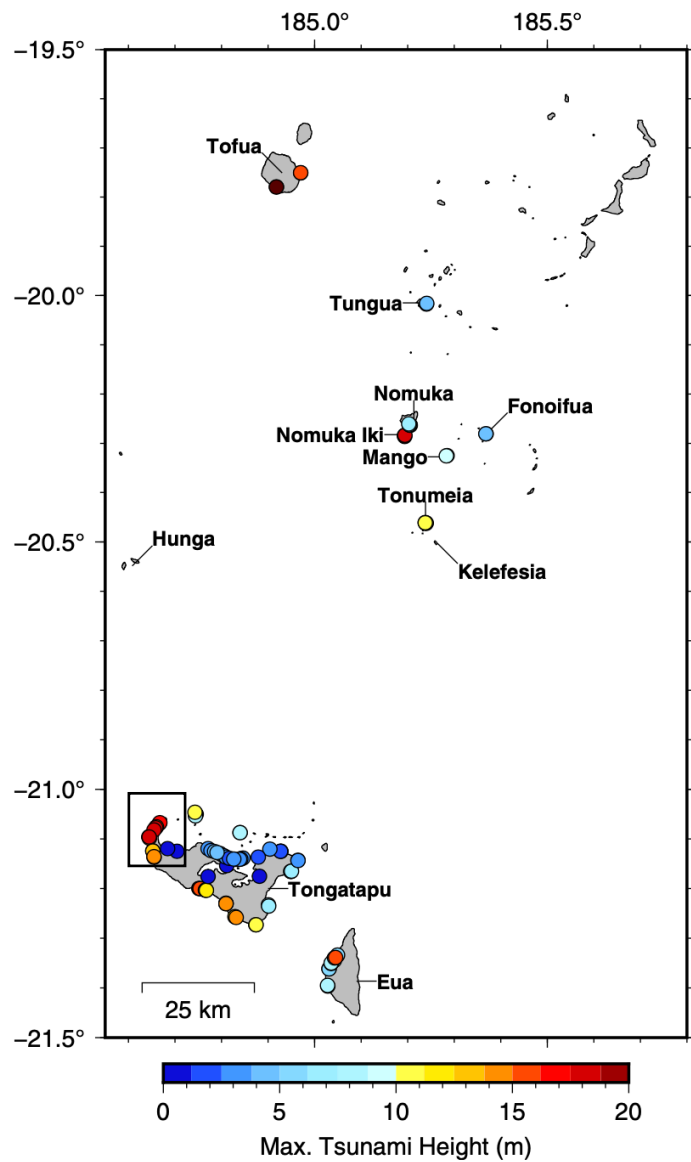
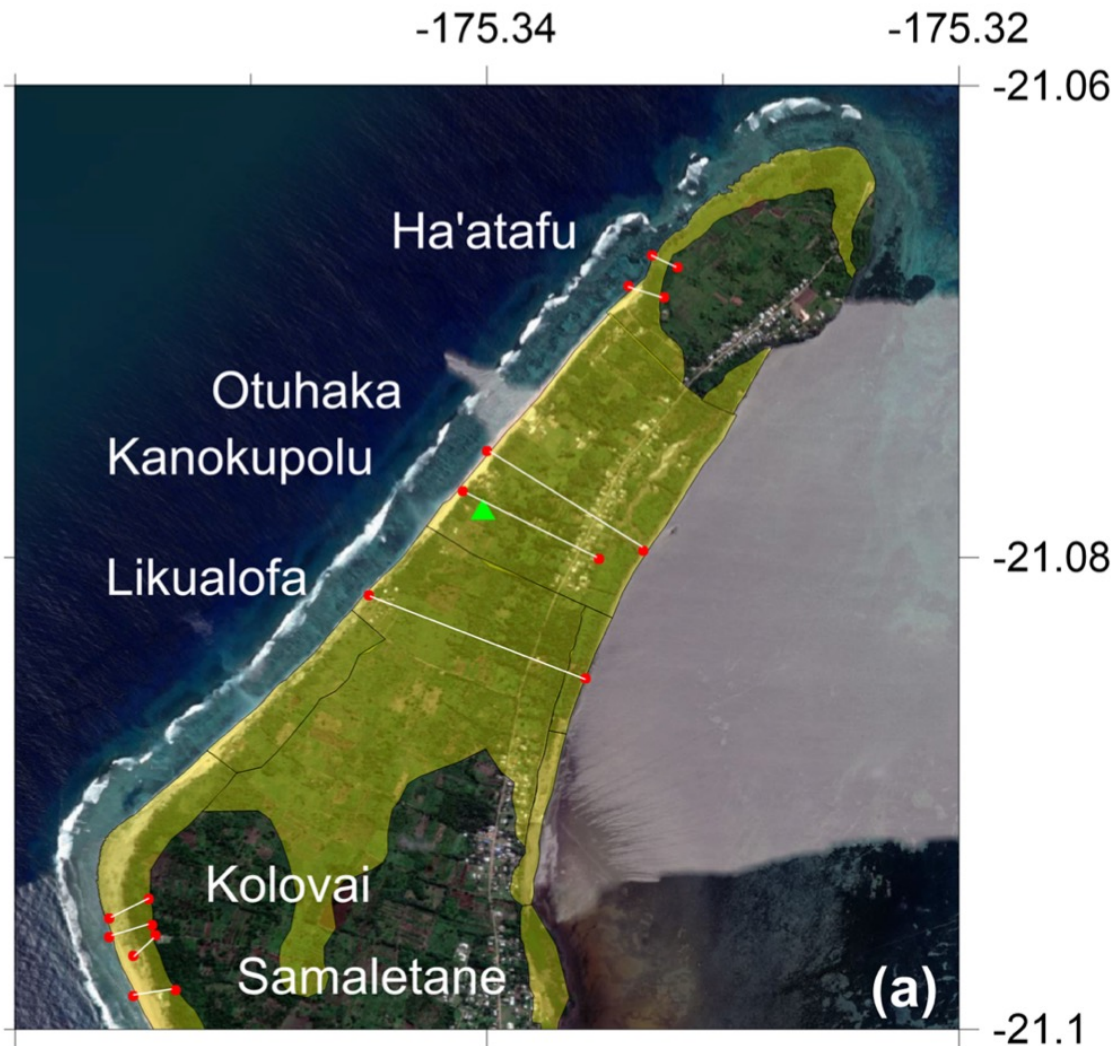
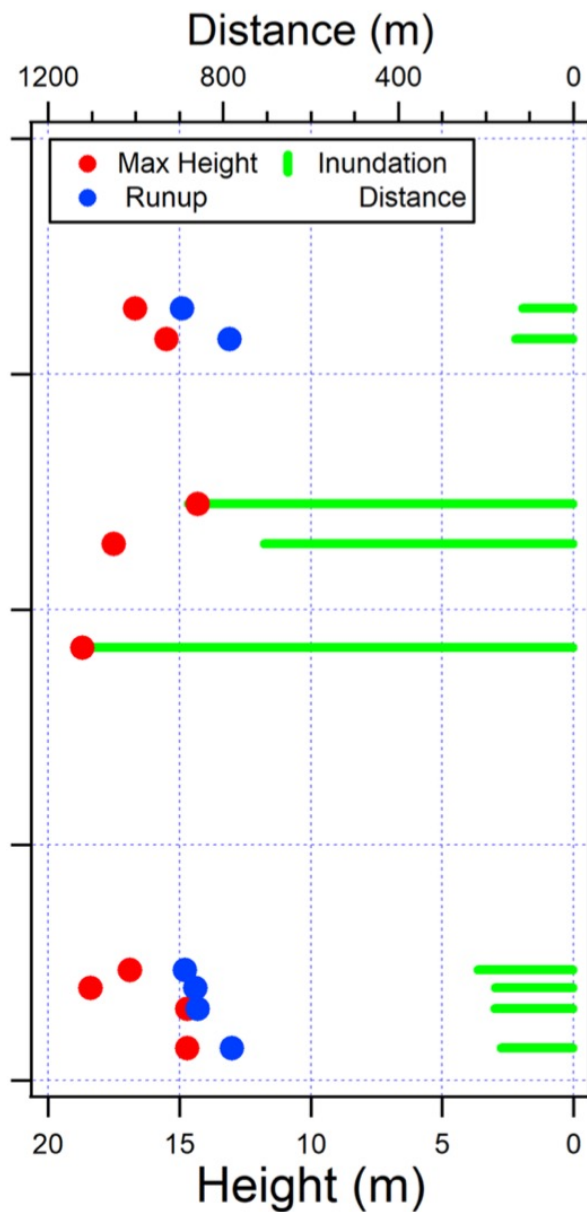


Figure 6
Summary data plots of maximum measured tsunami heights



Borrero et al. (2023)

Tsunami Damages

Tonga (Borrero et al., 2022)



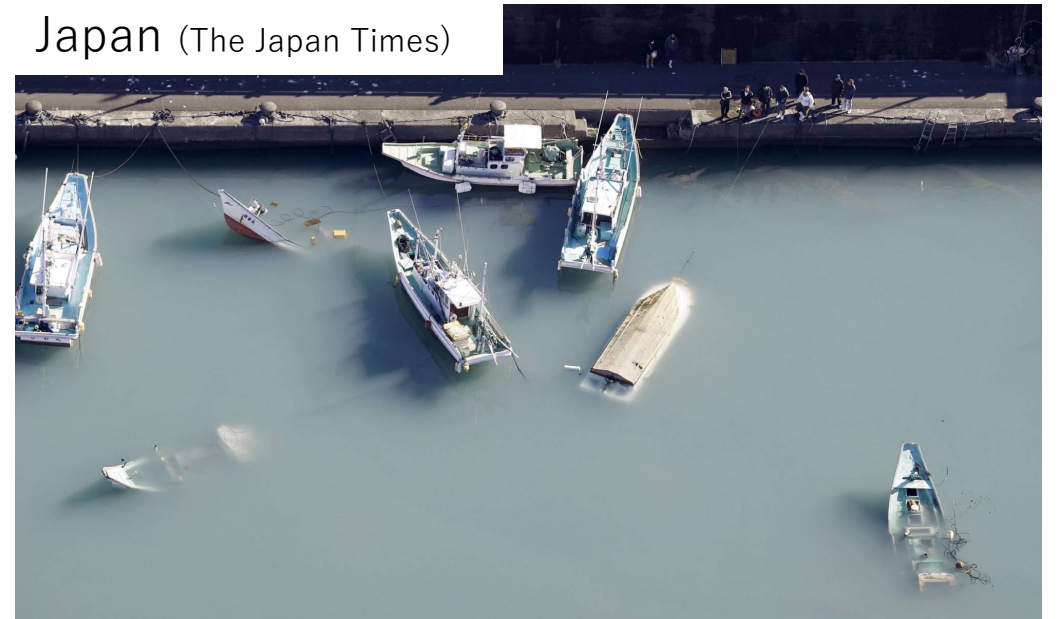
New Zealand (Stuff)



Peru (Merco Press)

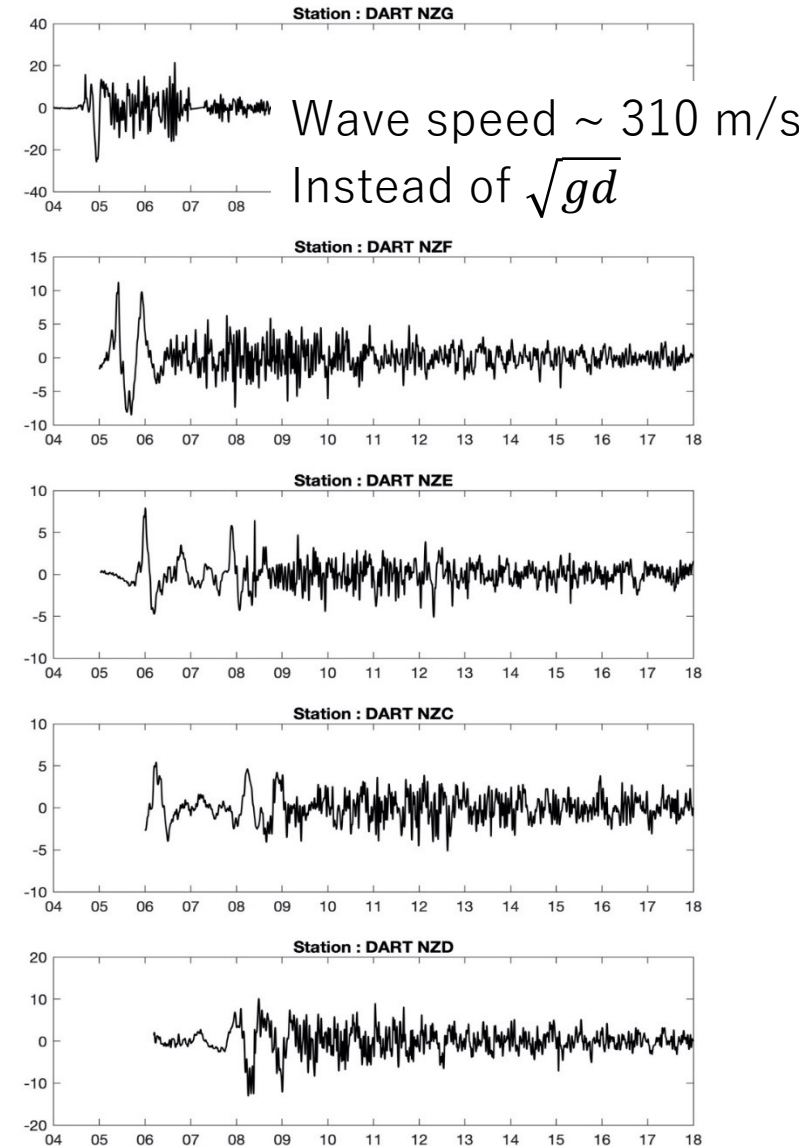
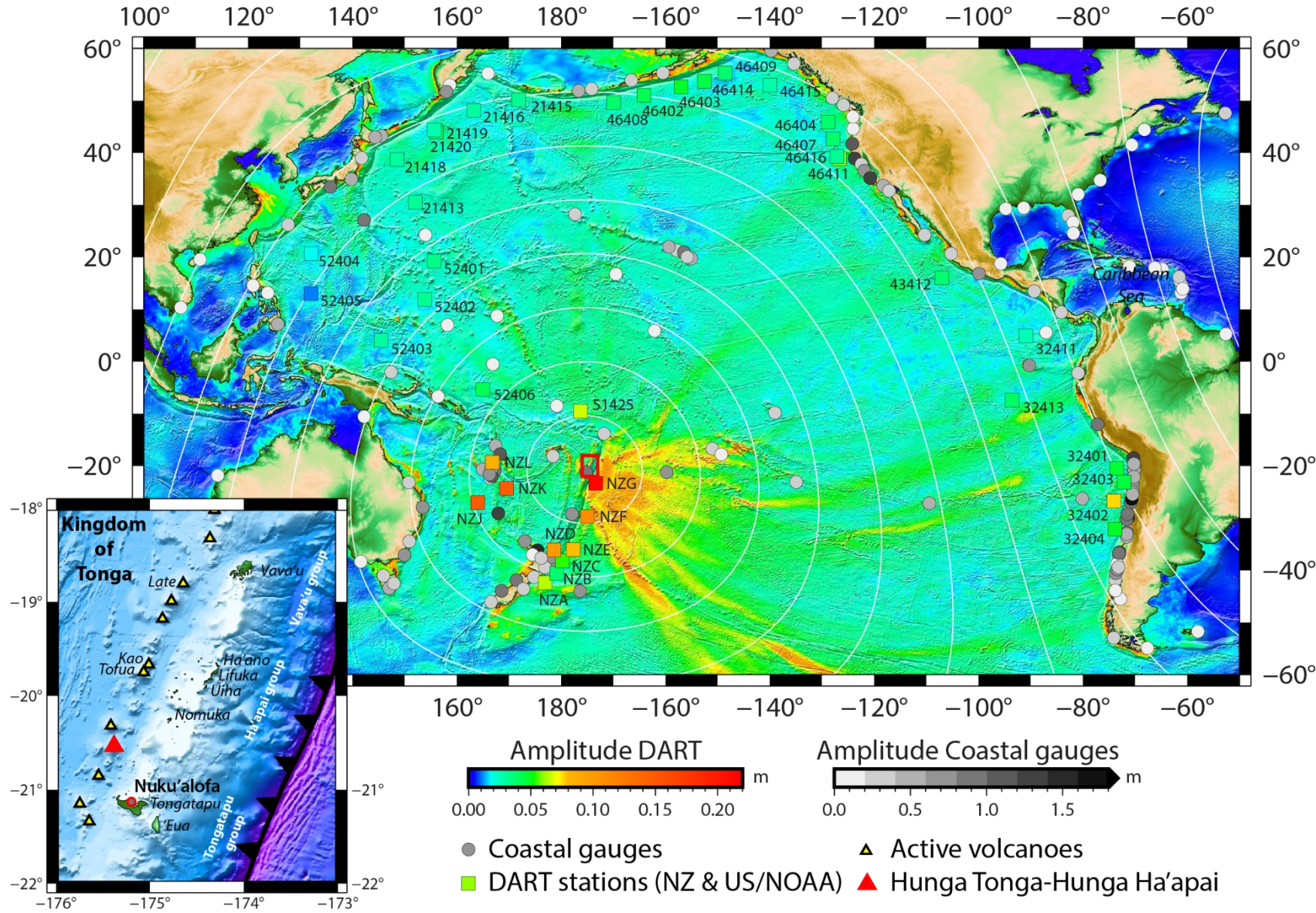


Japan (The Japan Times)



Sea level observations

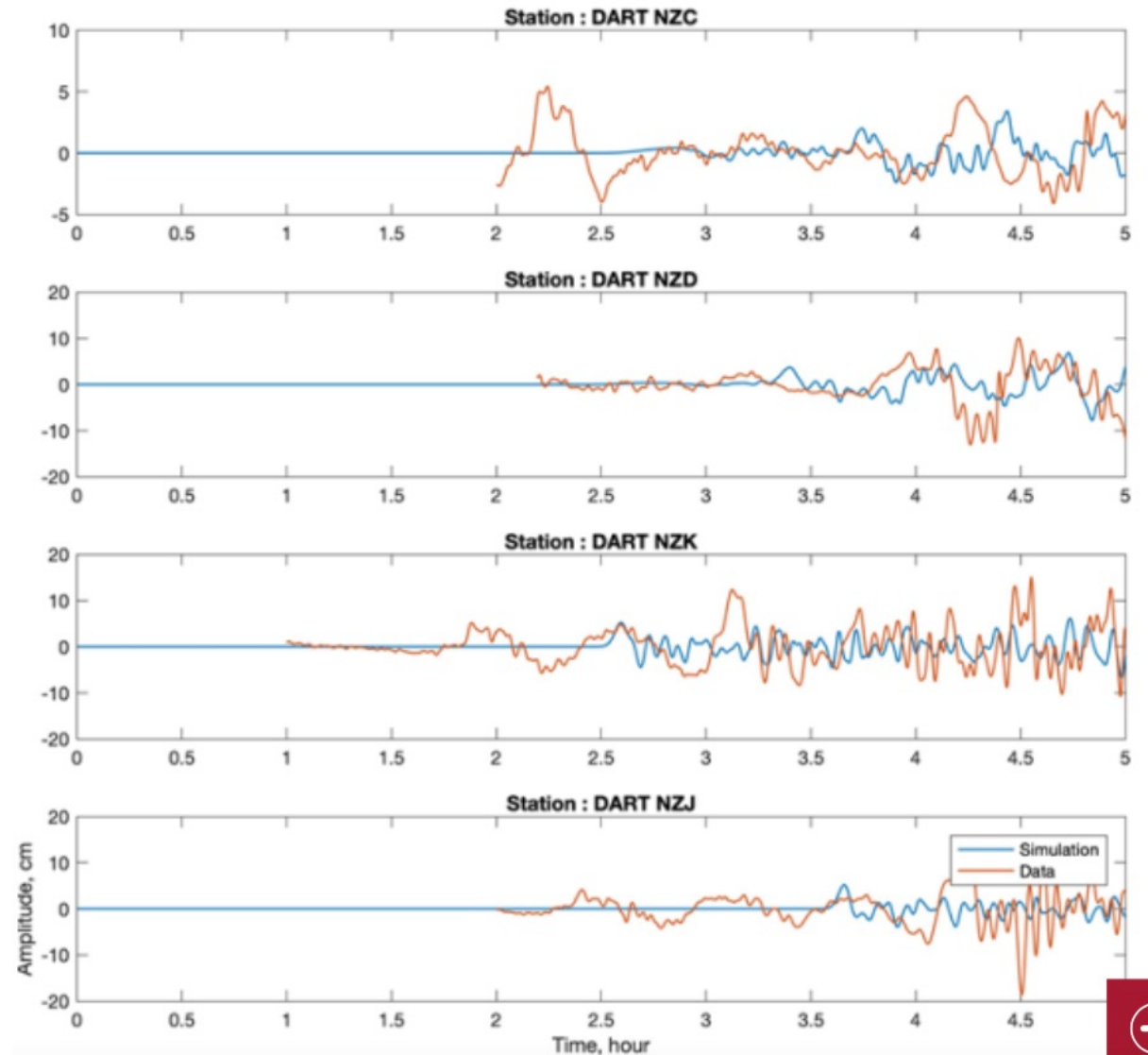
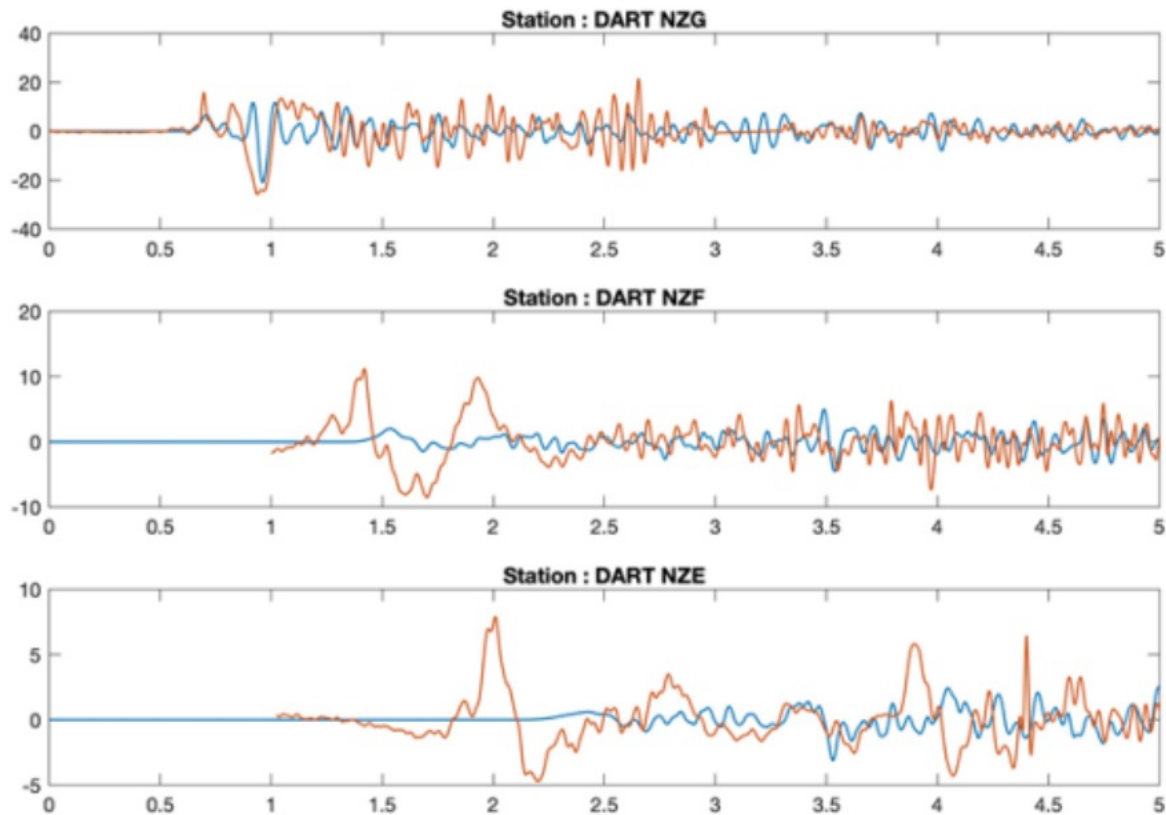
Bottom pressure gauge (DART): $p_{obs} = p_{atm} + p_{\eta}$



Gusman et al. (2022)

Initial Localized Tsunami Model

Localized tsunami source models can't reproduce the observed tsunami waveforms



Air-wave Generated Tsunami Simulation

The long wave theory can be used to simulate the behavior of air pressure waves in the atmosphere. The equations take into account factors such as atmospheric temperature, gravity, and air density.

$$\frac{\partial p}{\partial t} + \frac{\rho_a g}{R \sin \theta} \left[\frac{\partial [u_p H_p]}{\partial \varphi} + \frac{\partial [v_p H_p \sin \theta]}{\partial \theta} \right] = 0$$

$$\frac{\partial u_p}{\partial t} + \frac{1}{\rho_a R \sin \theta} \left[\frac{\partial p}{\partial \varphi} \right] + f v = 0$$

$$\frac{\partial v_p}{\partial t} + \frac{1}{\rho_a R} \left[\frac{\partial p}{\partial \theta} \right] - f u = 0$$

$$H_p = \frac{\gamma R T}{g M}$$

$\gamma = 1.4$; % ratio of specific heat of air

$T = 288$ % K

$R = 8314.36$; % J Kmol⁻¹ K⁻¹ universal gas constant

$M = 28.966$; % kg Kmol⁻¹ Molecular mass for dry air

$g = 9.81$; % gravity acceleration m s⁻²

$\rho_a = 1.225$; % air density in 15C in kg m⁻³ (Amores et al., 2022)

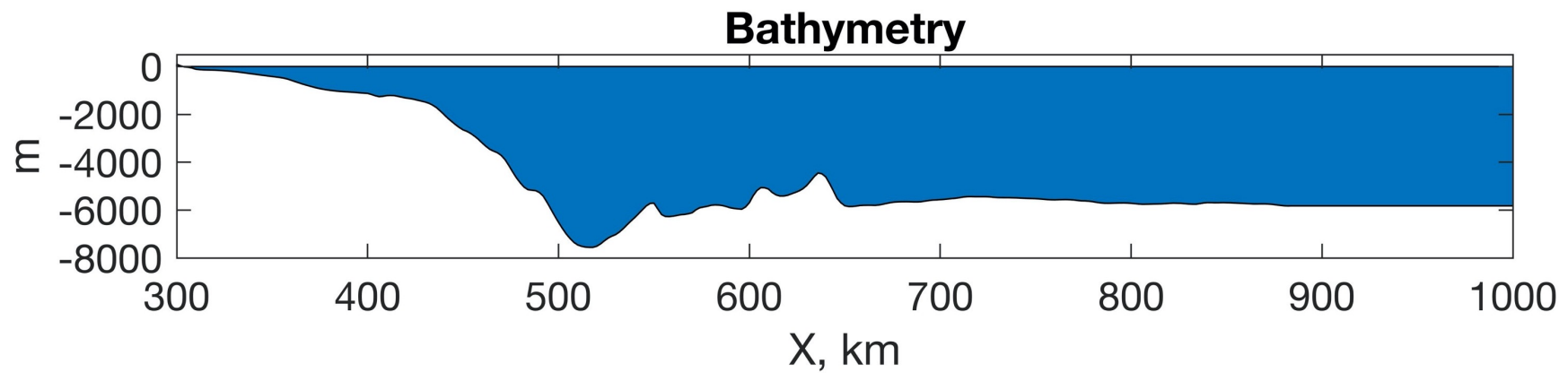
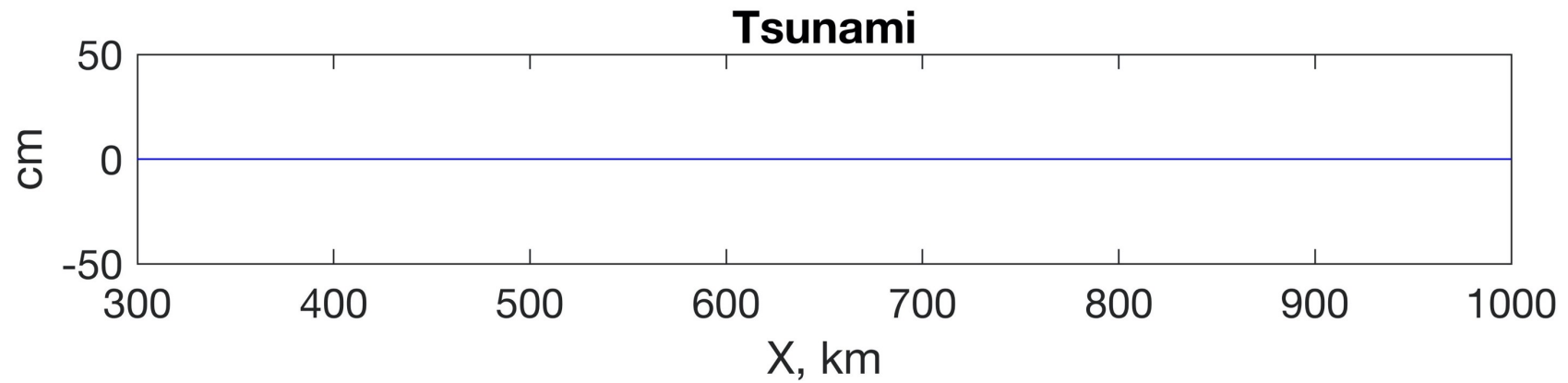
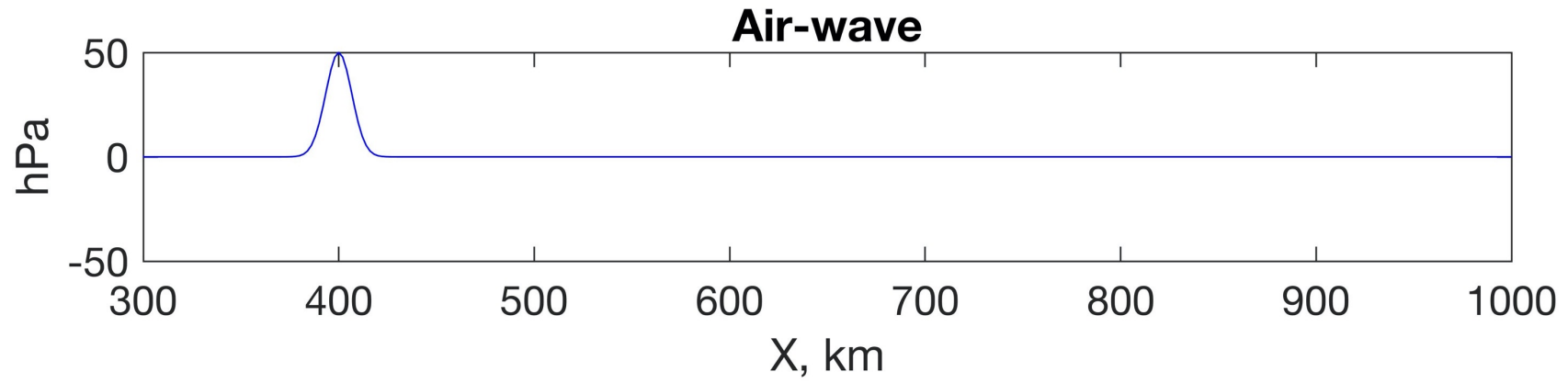
To simulate the tsunami generated by the air wave we used a linear shallow water wave model with the atmospheric pressure term in spherical coordinates

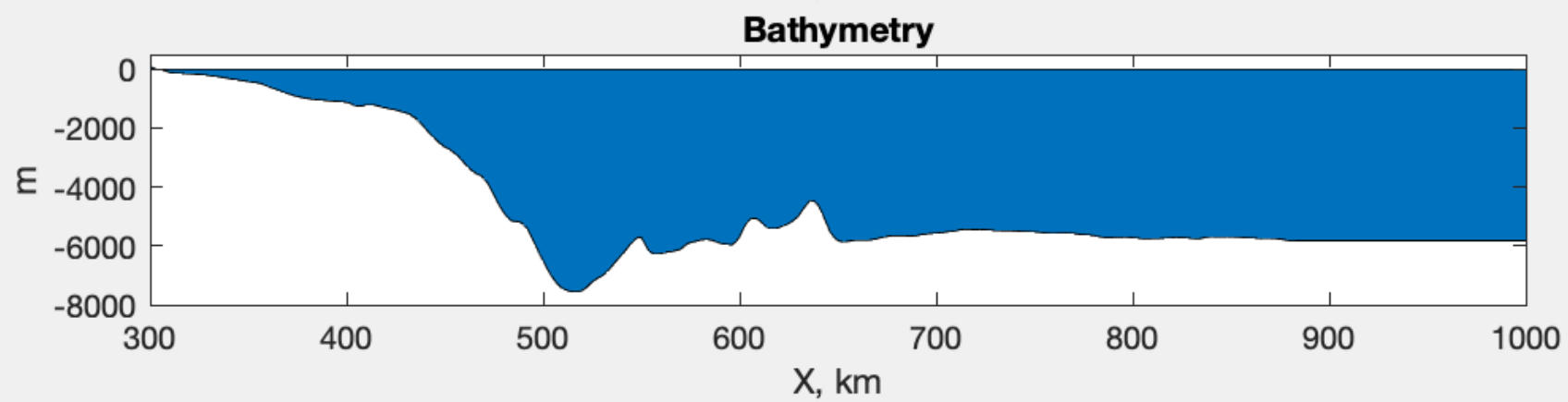
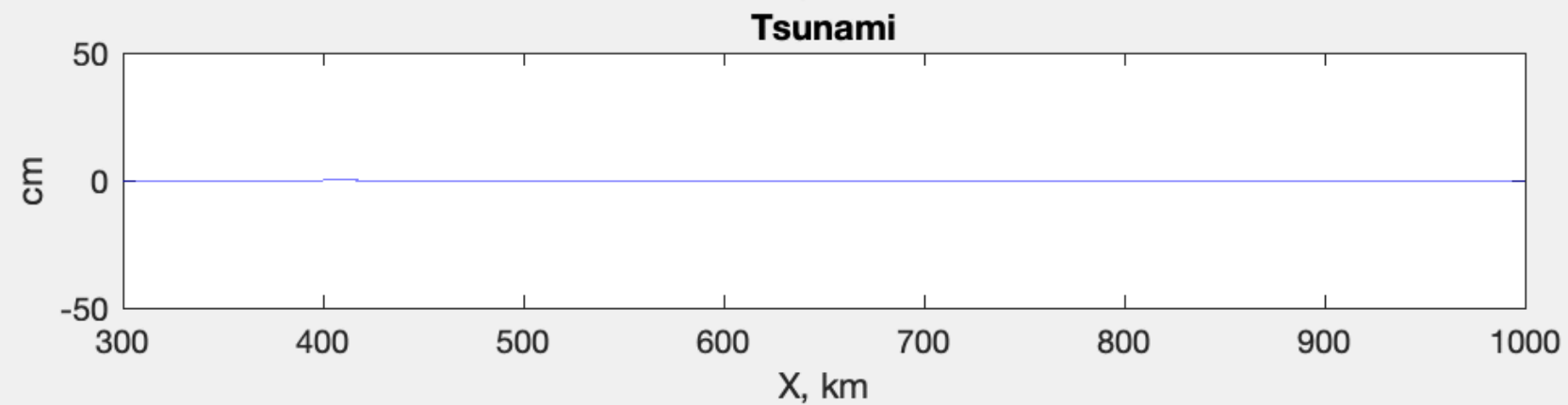
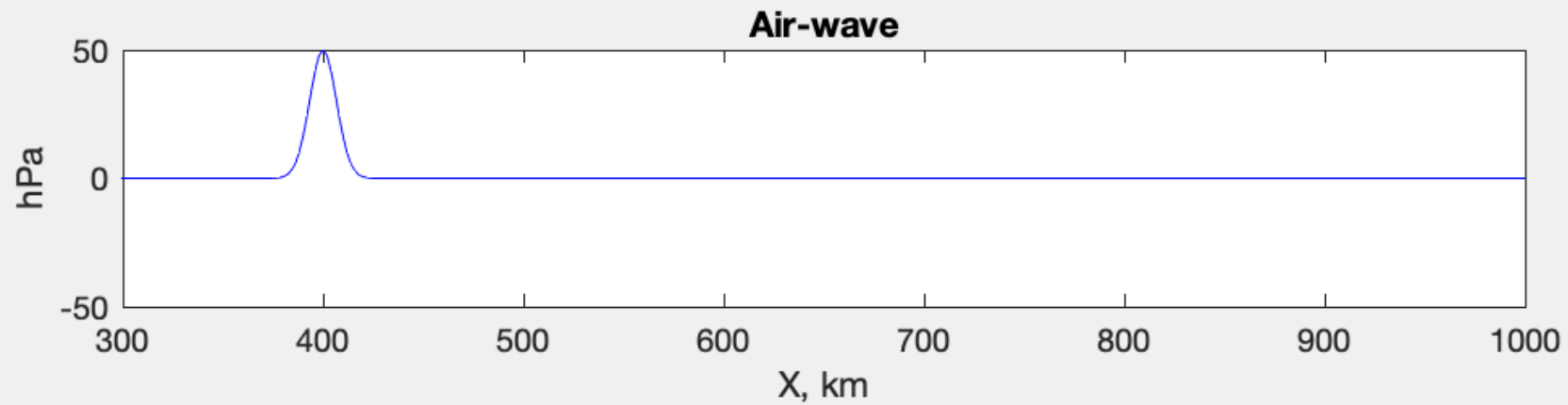
$$\frac{\partial h}{\partial t} + \frac{1}{R \sin \theta} \left[\frac{\partial [u d]}{\partial \varphi} + \frac{\partial [v d \sin \theta]}{\partial \theta} \right] = 0$$

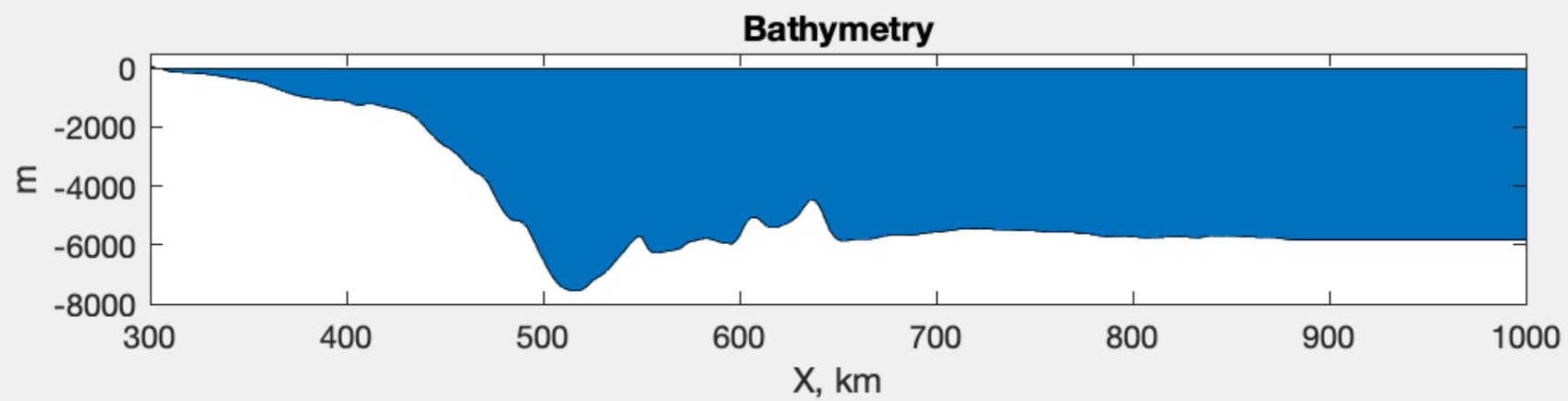
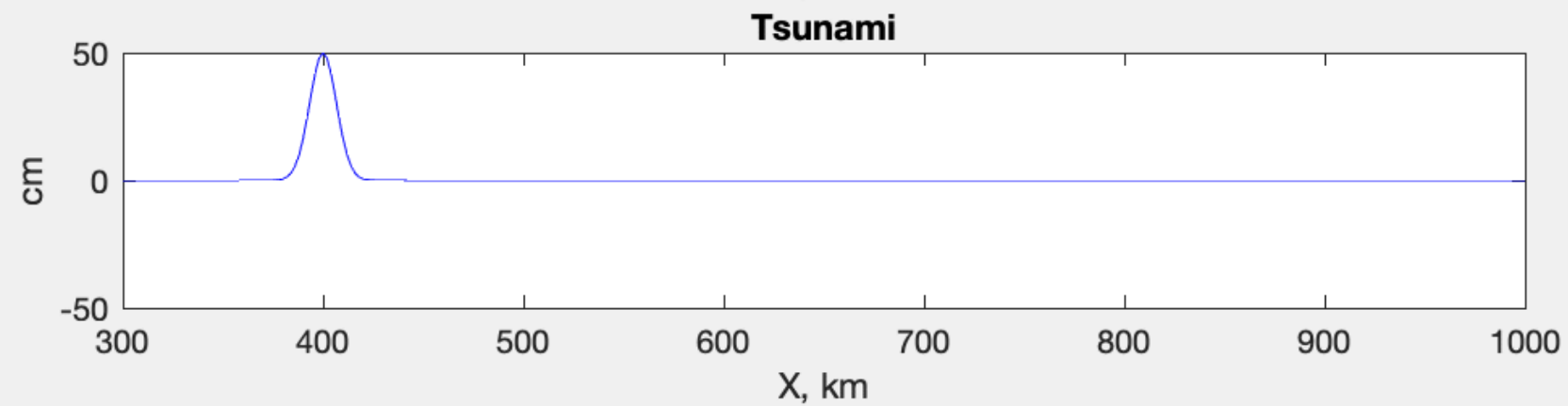
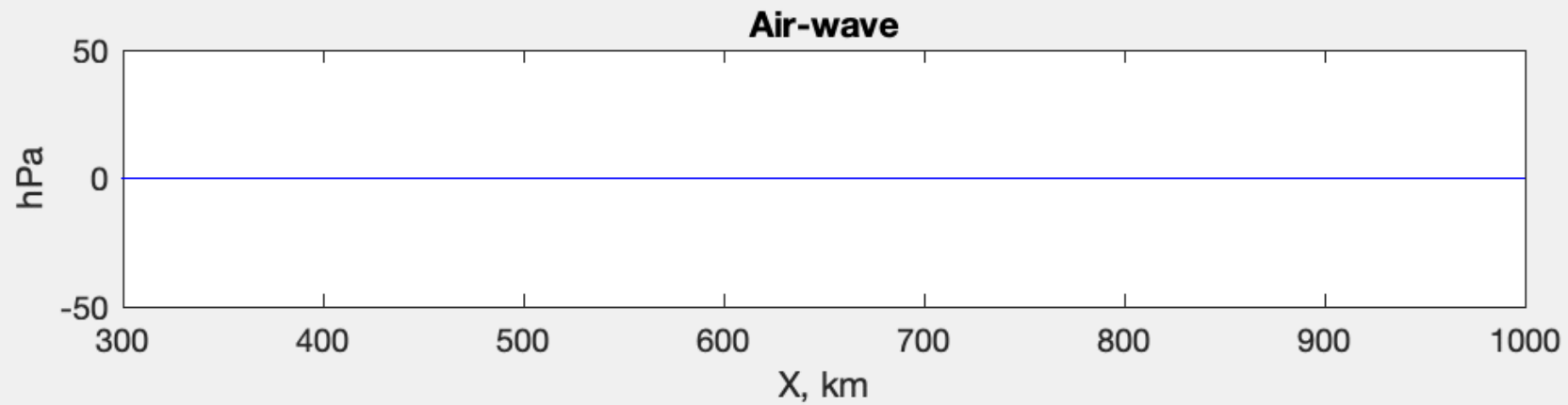
$$\frac{\partial u}{\partial t} + \frac{1}{R \sin \theta} \left[g \frac{\partial h}{\partial \varphi} + \frac{1}{\rho} \frac{\partial p}{\partial \varphi} \right] + f v = 0$$

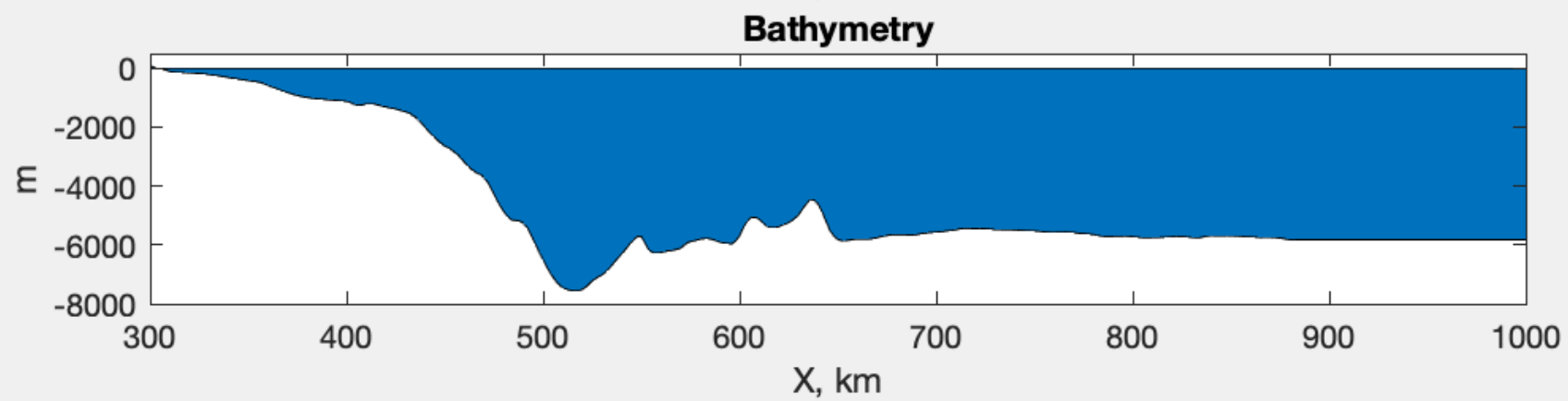
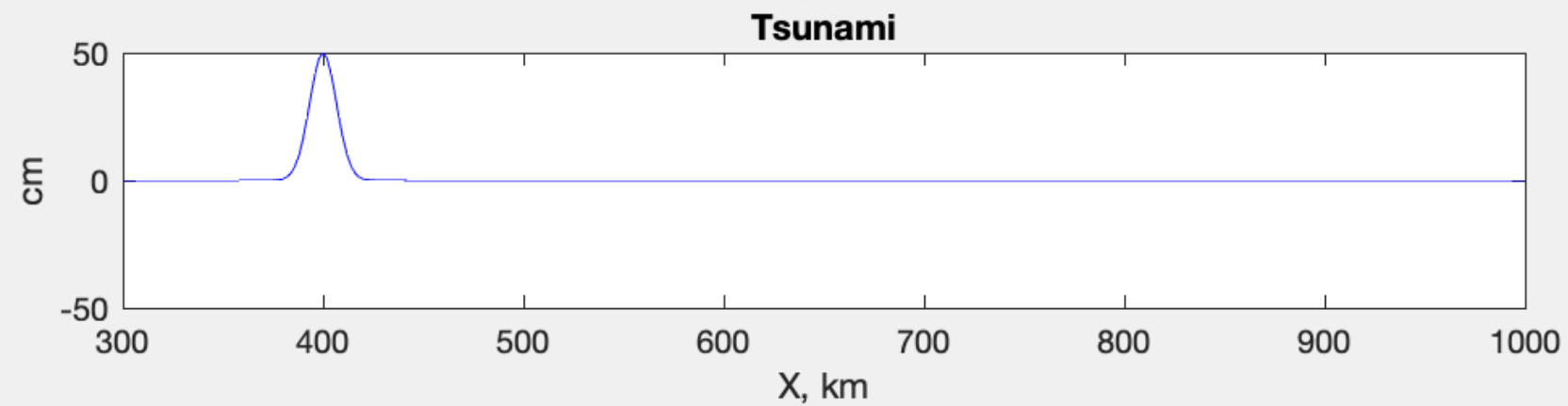
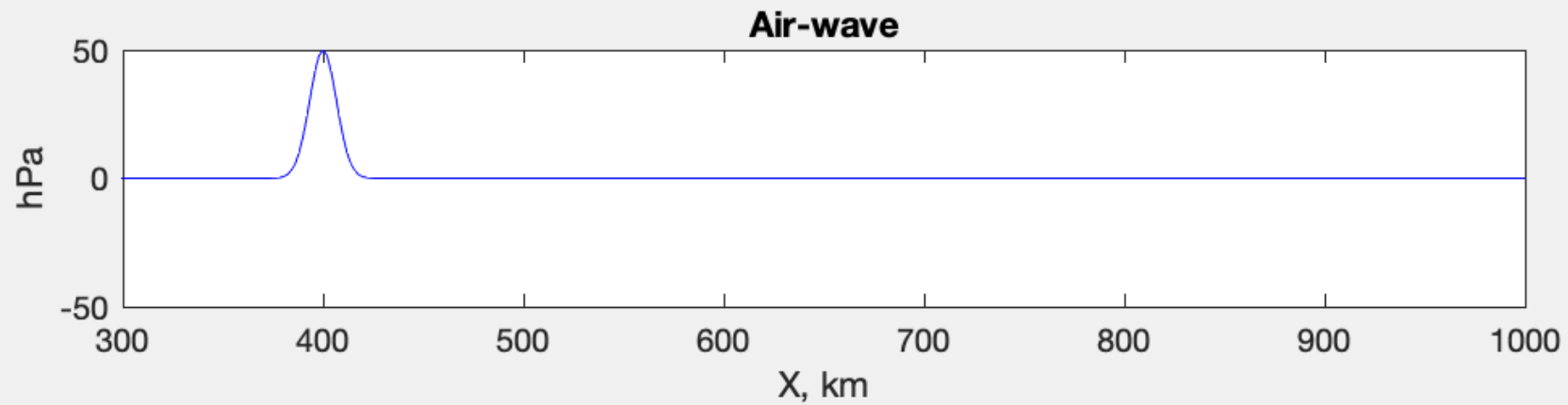
$$\frac{\partial v}{\partial t} + \frac{1}{R} \left[g \frac{\partial h}{\partial \theta} + \frac{1}{\rho} \frac{\partial p}{\partial \theta} \right] - f u = 0$$

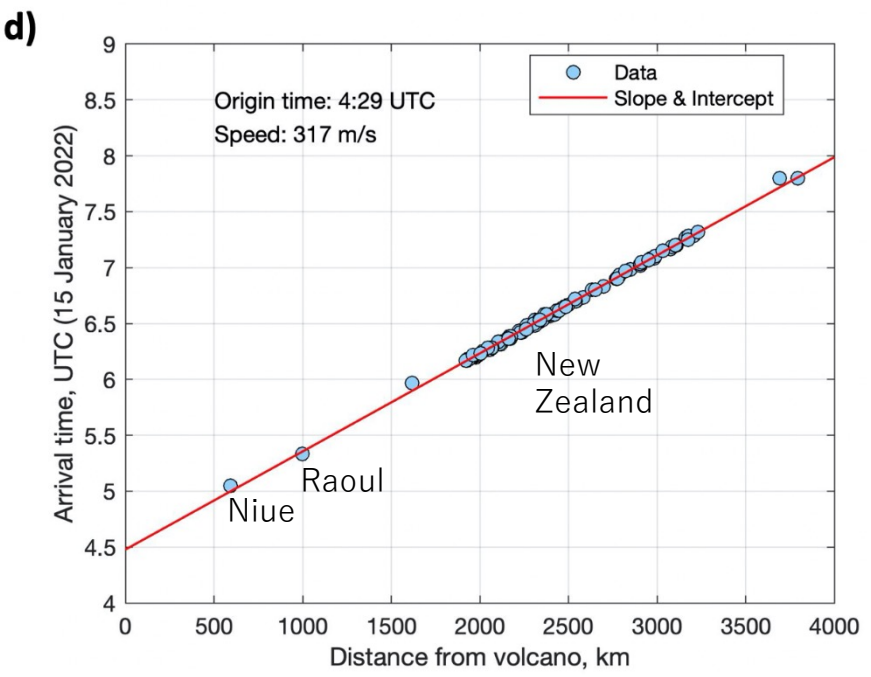
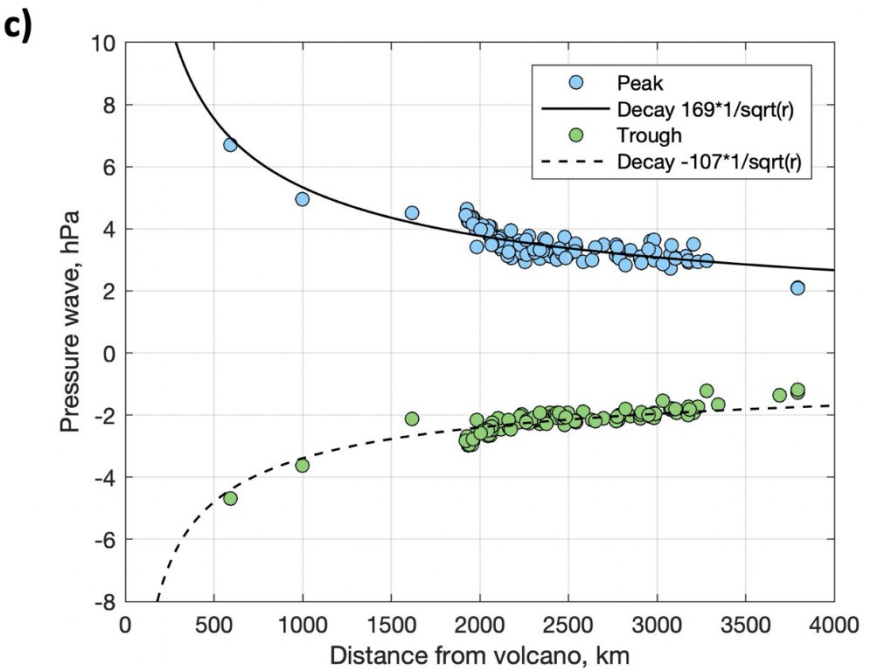
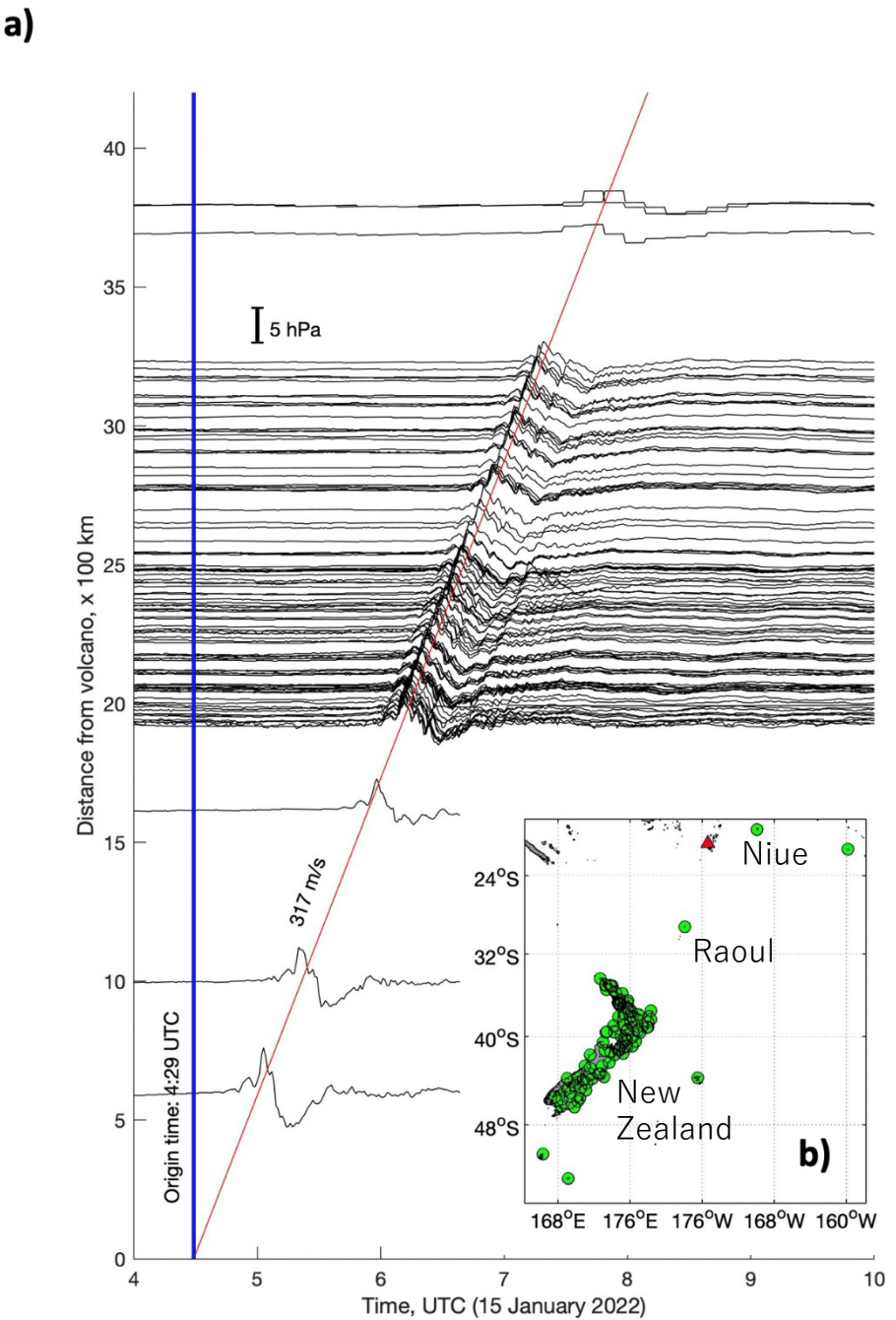
$$p_{obs} = p_{atm} + p_{\eta}$$











Air pressure observations

- Air pressure data at 94 stations (600 – 4000 km from HTHH volcano) were provided by MetService.
- Air-wave amplitude decays proportionately to $1/\sqrt{r}$.
- Estimated wave speed: **317 m/s**.
- Effective origin time: **4:29 UTC**.
- We used the above information to make a simple air pressure wave model.

Gusman et al. (2022)

Simple Air-wave Model

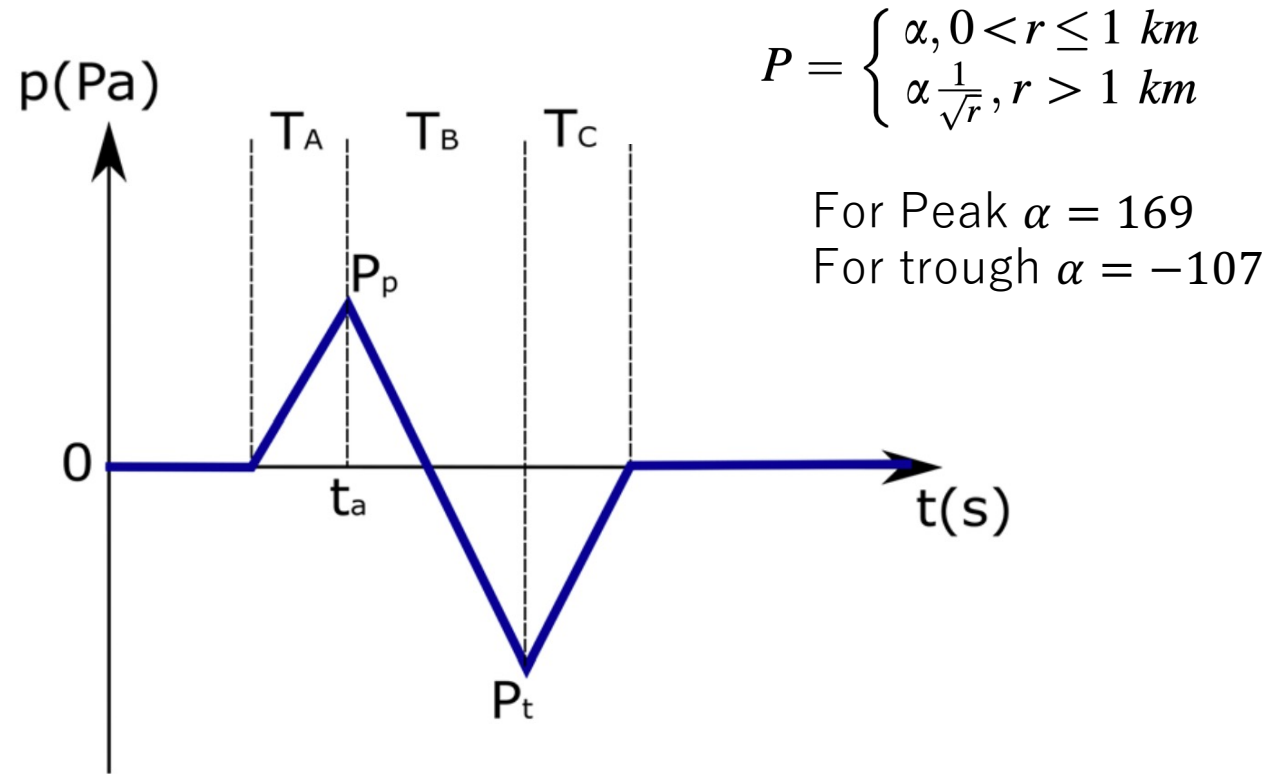
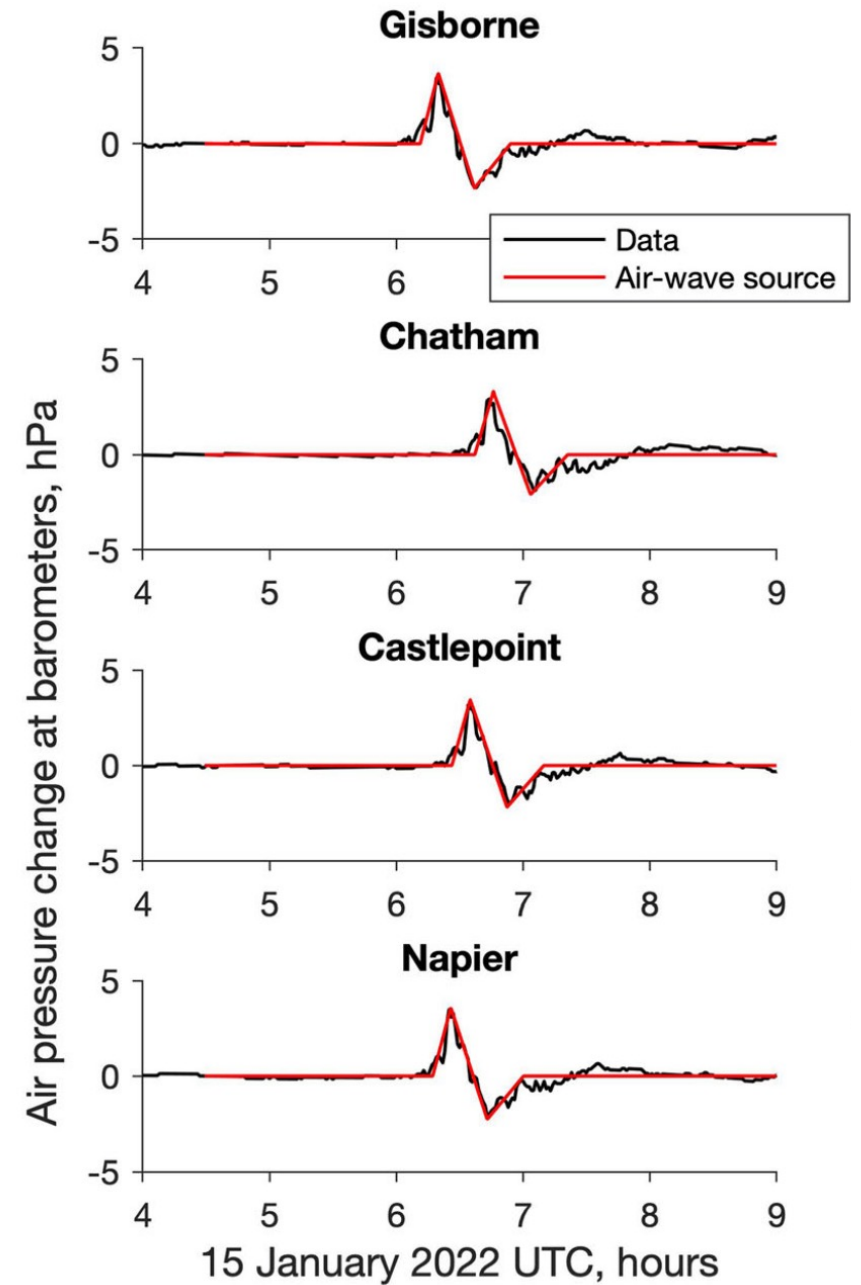
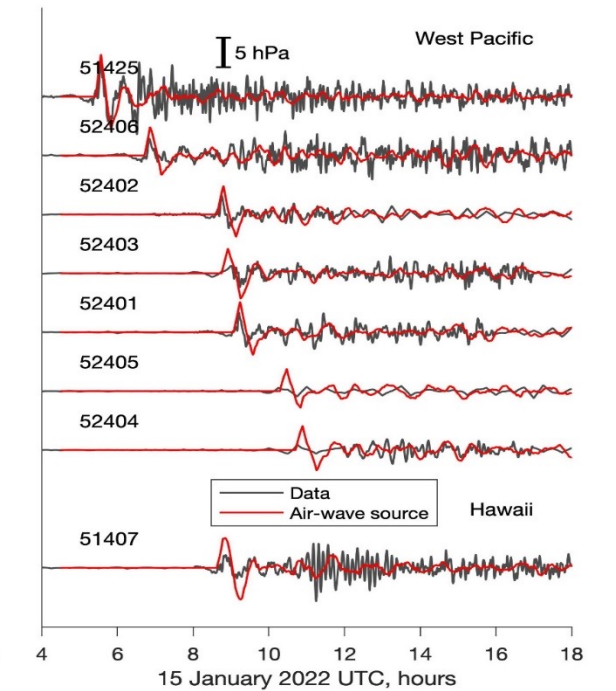
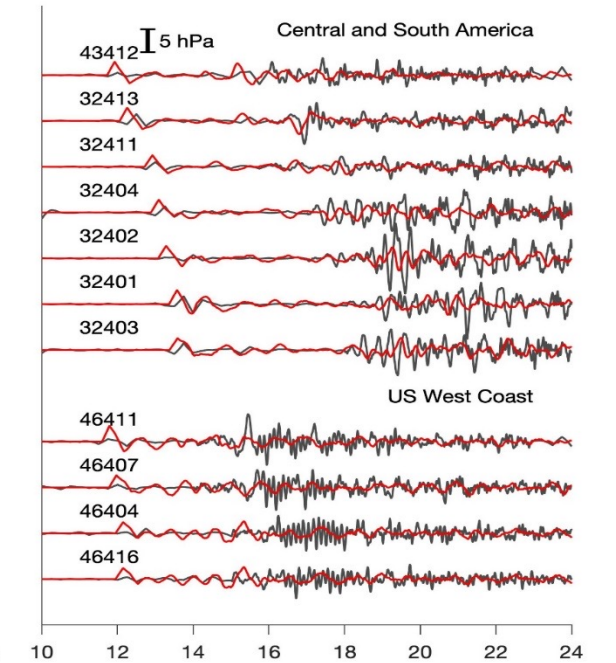
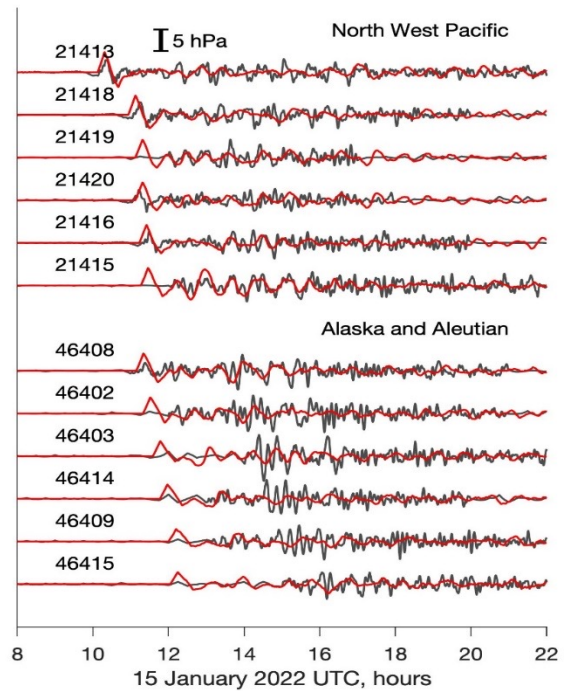
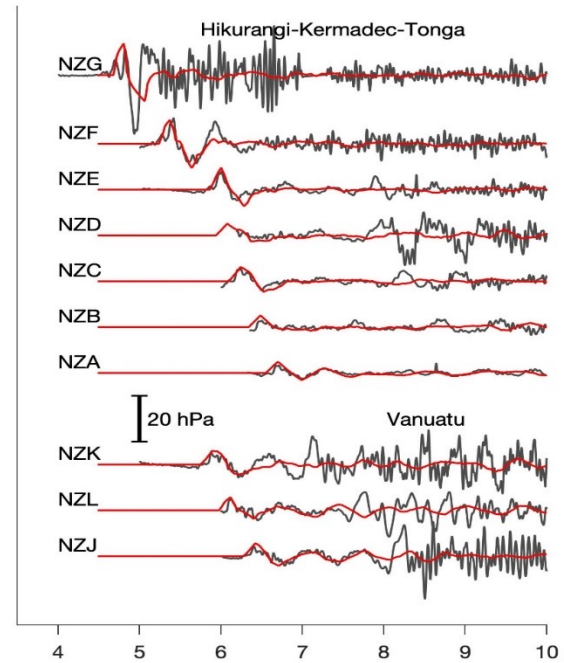
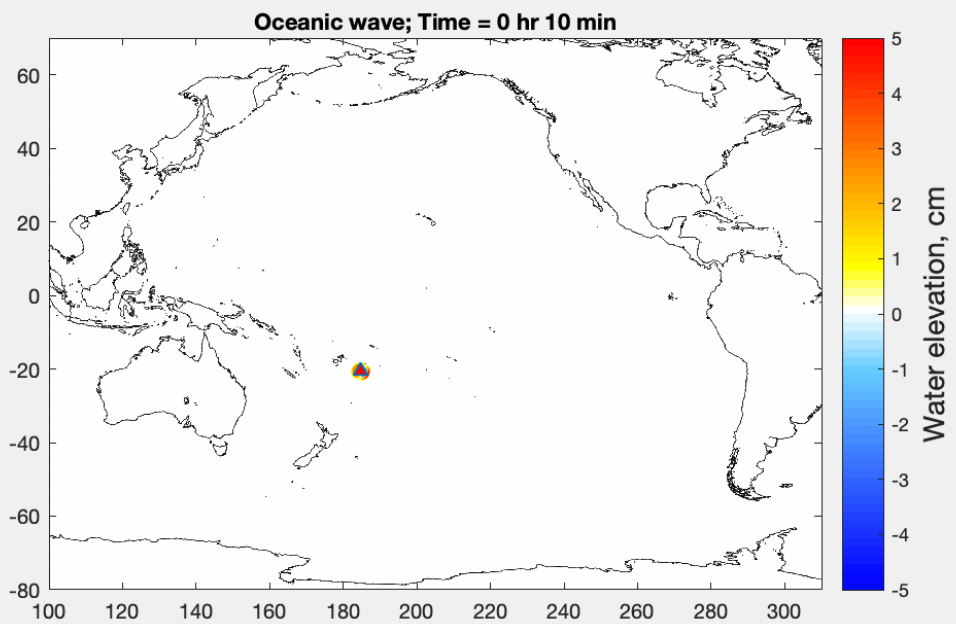
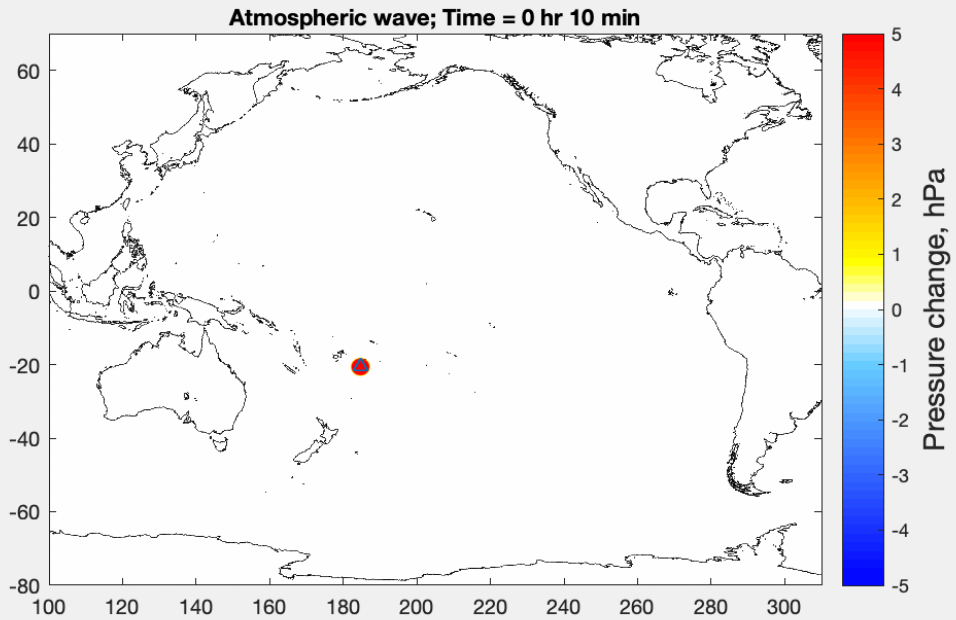


Figure 4

Illustration of air pressure wave model parameters used in this study





Gusman et al. (2022)

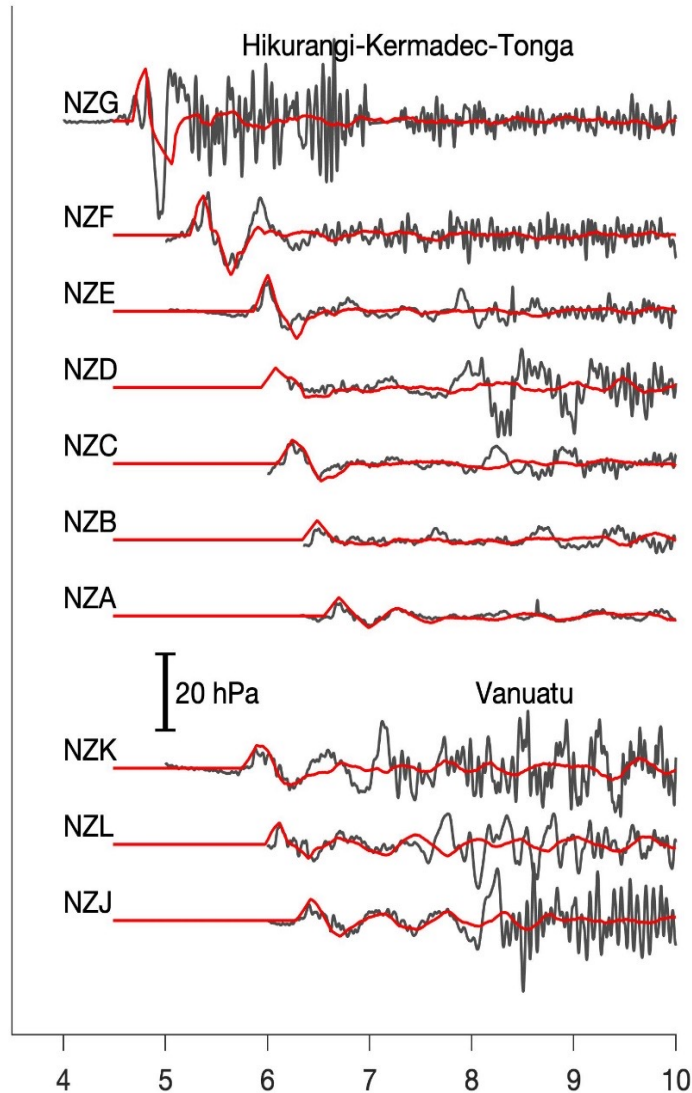
Localized Source

Volcanic tsunami source mechanisms according to Paris et al. (2014):

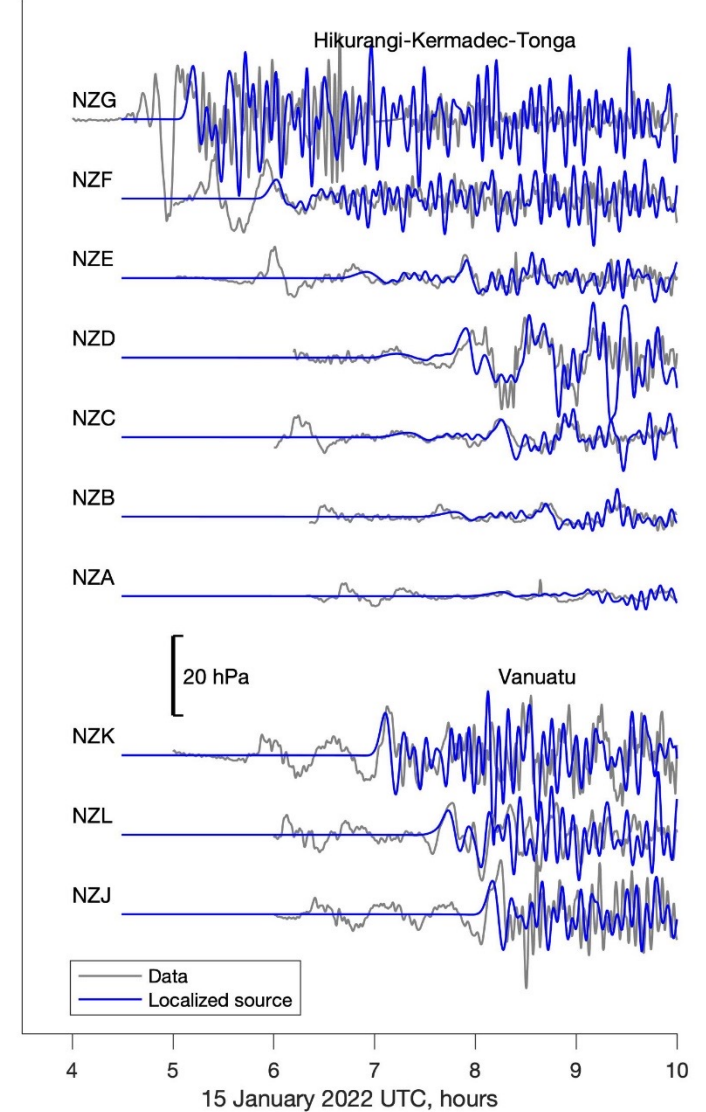
1. Underwater explosion
2. Air wave
3. Pyroclastic flow
4. Flank Failure
5. Caldera subsidence
6. Lahar
7. Earthquake

Localized source: A circular water uplift at the volcano with a characteristic diameter of 10 km and the same origin time as the air-wave

Air wave Continuously propagating source



Water displacement Localized source



Gusman et al. (2022)

Article Contents

Summary

JOURNAL ARTICLE ACCEPTED MANUSCRIPT

Source estimation of the tsunami later phases associated with the 2022 Hunga Tonga volcanic eruption


Ayumu Mizutani , Kiyoshi Yomogida


Geophysical Journal International, ggad174, <https://doi.org/10.1093/gji/ggad174>


Published: 21 April 2023




PDF

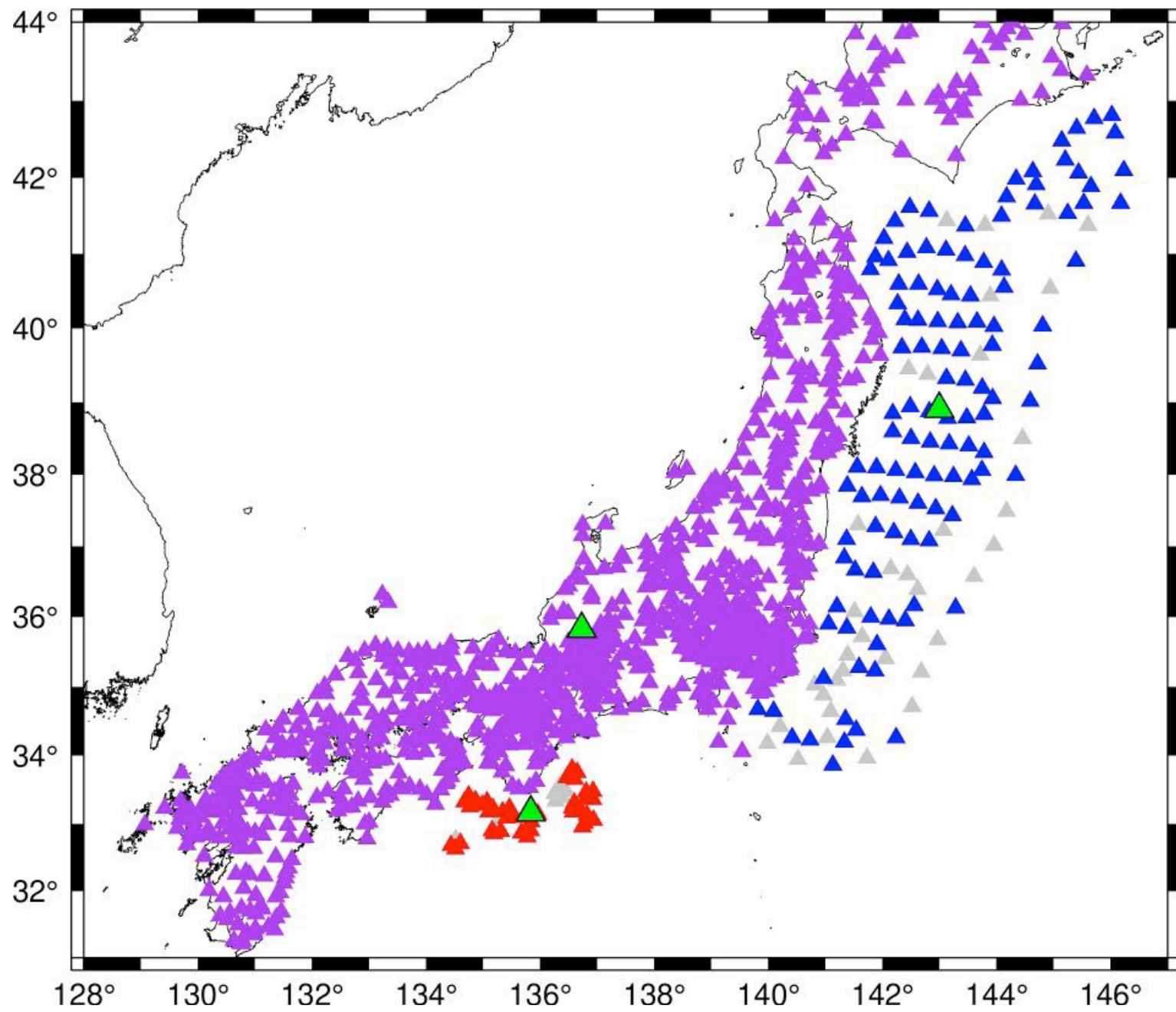
 Split View

 Cite

 Permissions

 Share ▼

Summary



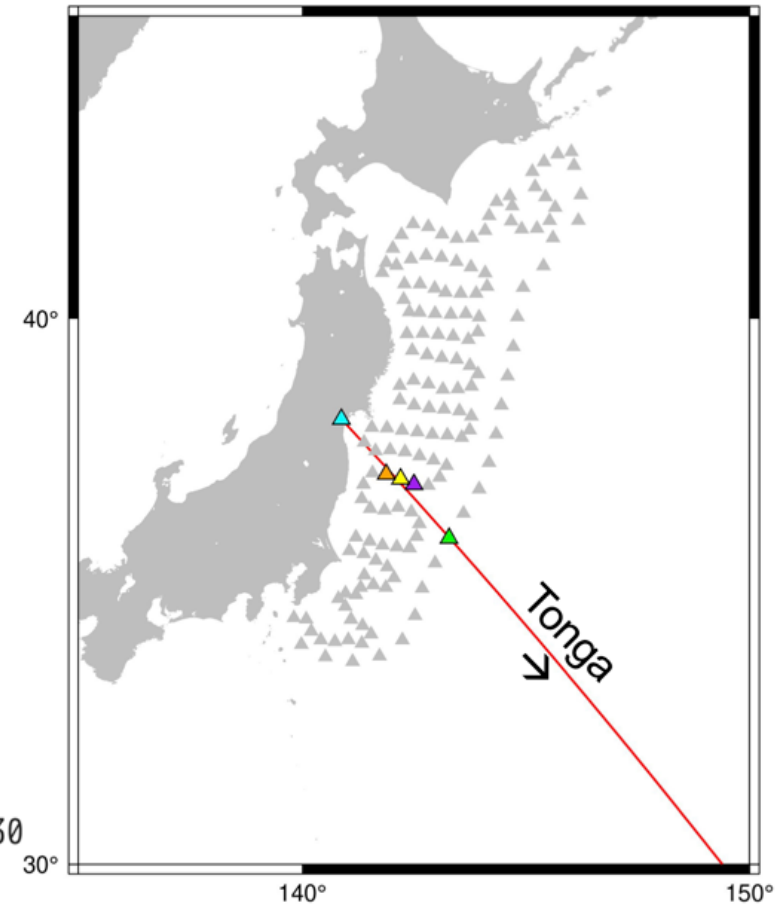
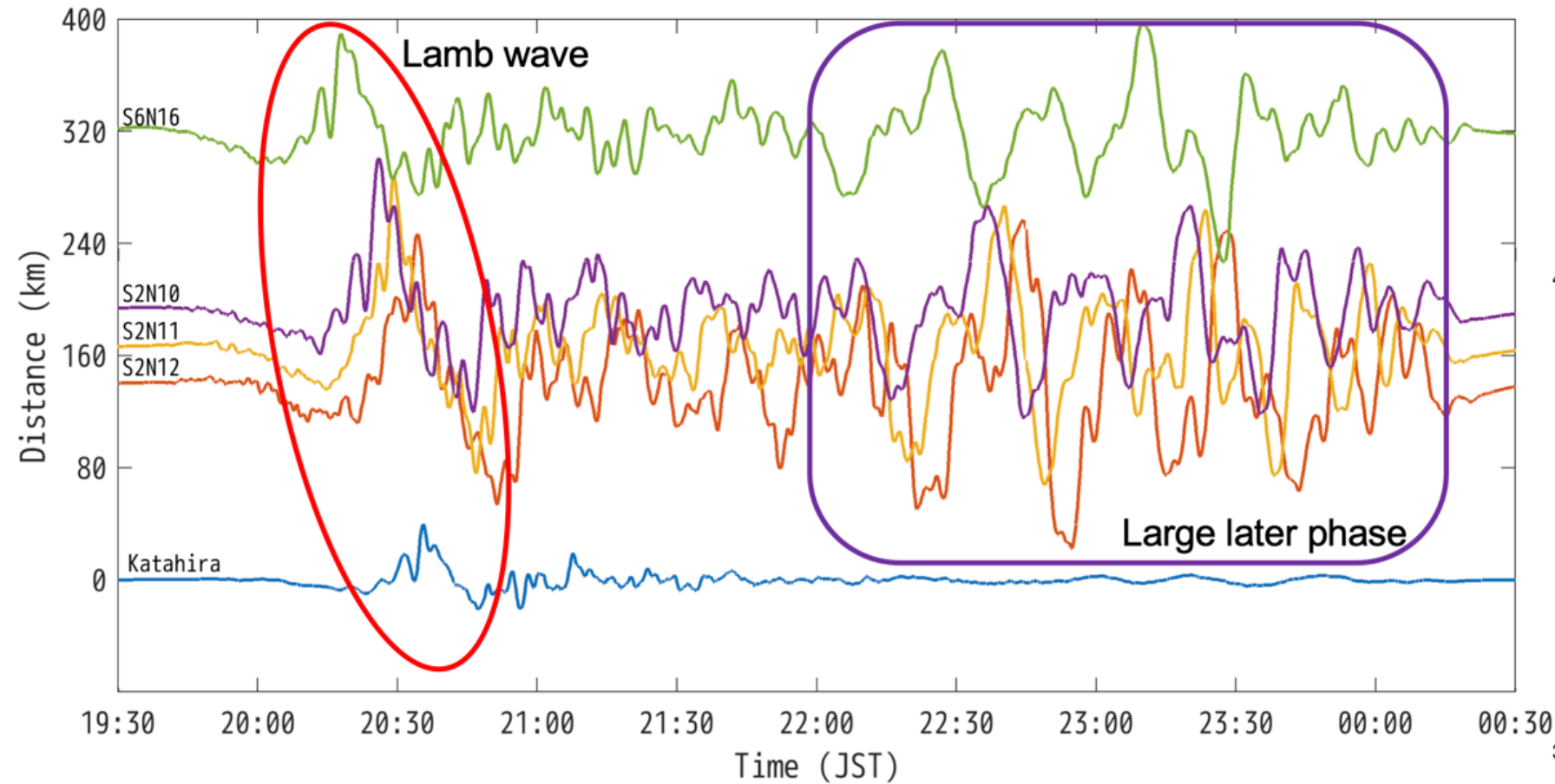


Figure: Observation records of four OBP gauges and a barometer aligned along with the great circle from Tonga Island. The colors of each waveform represent the station on the right-hand side map. Note that station Katahira is a barometer while stations S2N12, S2N11, S2N10, and S6N16 are OBP gauges.

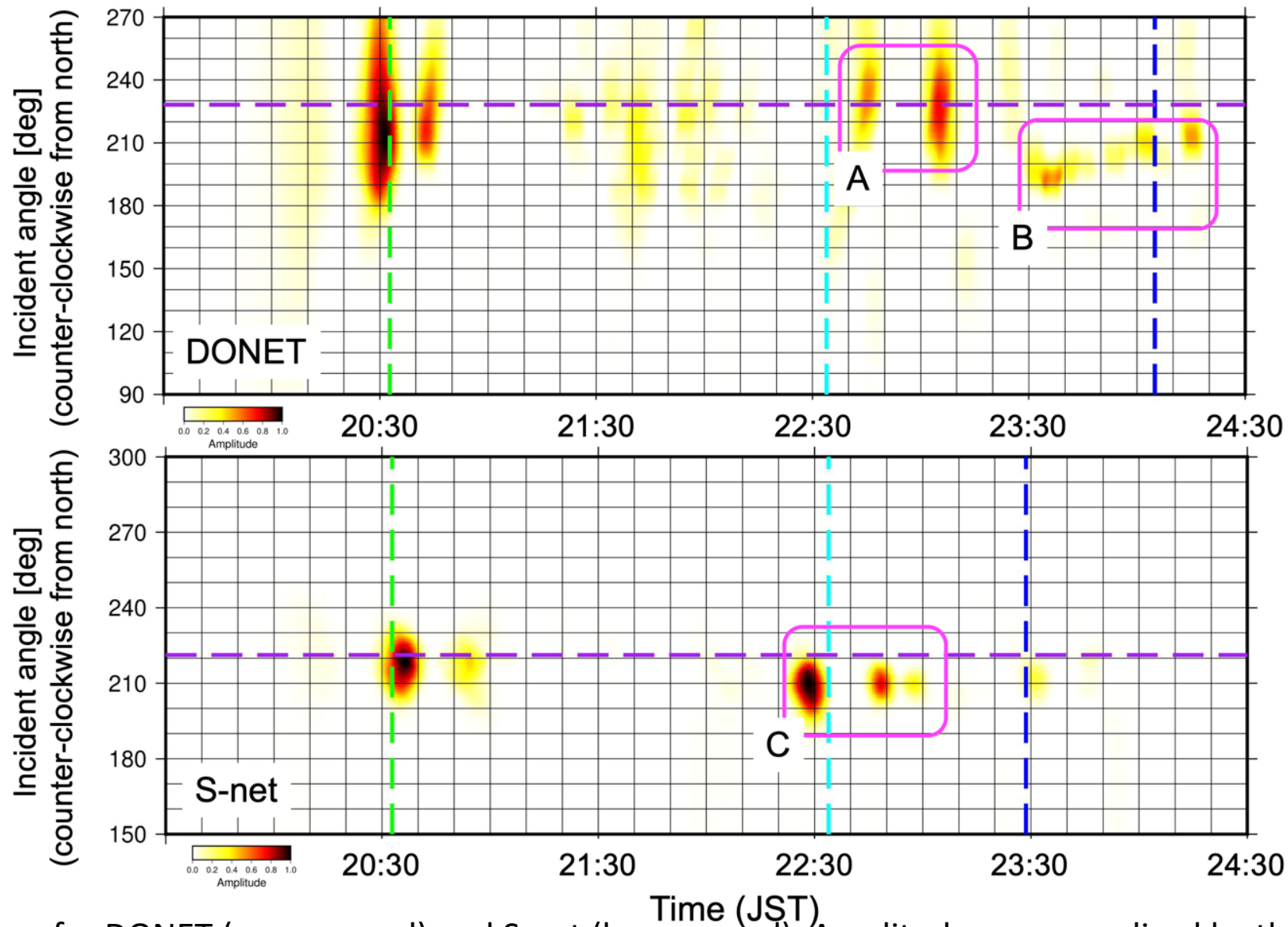


Figure: Vespagrams for DONET (upper panel) and S-net (lower panel). Amplitudes are normalized by the maximum value of each plot. The purple line represents the incident angle of the great circle path from Tonga Island to the reference points of each network. The green and cyan lines give the arrival times of the waves along the great circle with speeds of 300 m/s and 235 m/s, respectively. The blue line represents the theoretical tsunami arrival time from Tonga Island.

4.5.1 Finite difference method

For atmospheric and oceanic waves, we solved their equations of motions in the spherical coordinate formulated by Kubota et al. (2022). For atmospheric waves,

$$\begin{aligned}\frac{\partial p_{atm}}{\partial t} + \frac{K}{R \cos \theta} \left[\frac{\partial v_{\lambda}}{\partial \lambda} + \frac{\partial (v_{\theta} \cos \theta)}{\partial \theta} \right] &= \frac{\partial p_s}{\partial t}, \\ \frac{\partial v_{\lambda}}{\partial t} &= -\frac{1}{\rho_a R \cos \theta} \frac{\partial p_{atm}}{\partial \lambda}, \\ \frac{\partial v_{\theta}}{\partial t} &= -\frac{1}{\rho_a R} \frac{\partial p_{atm}}{\partial \theta},\end{aligned}\tag{4.4}$$

where p_{atm} is the atmospheric pressure disturbance, K is the bulk modulus, v_{λ} and v_{θ} are the velocities of the atmosphere in the directions of longitude λ and latitude θ , R is the Earth's radius, ρ_a is the atmospheric density, and p_s represents the pressure at the source, respectively. For tsunami waves,

$$\begin{aligned}\frac{\partial \eta}{\partial t} + \frac{1}{R \cos \theta} \left[\frac{\partial (hu_{\lambda})}{\partial \lambda} + \frac{\partial (hu_{\theta} \cos \theta)}{\partial \theta} \right] &= 0, \\ \frac{\partial u_{\lambda}}{\partial t} &= -\frac{g}{R \cos \theta} \frac{\partial \eta}{\partial \lambda} - \frac{1}{\rho_w R \cos \theta} \frac{\partial p_{atm}}{\partial \lambda}, \\ \frac{\partial u_{\theta}}{\partial t} &= -\frac{g}{R} \frac{\partial \eta}{\partial \theta} - \frac{1}{\rho_w R} \frac{\partial p_{atm}}{\partial \theta},\end{aligned}\tag{4.5}$$

where η is the tsunami height, h is the sea depth, u_{λ} and u_{θ} are the velocities of the ocean in the directions of longitude and latitude, g is the gravitational acceleration, and ρ_w is the water density. Note that, in this study,

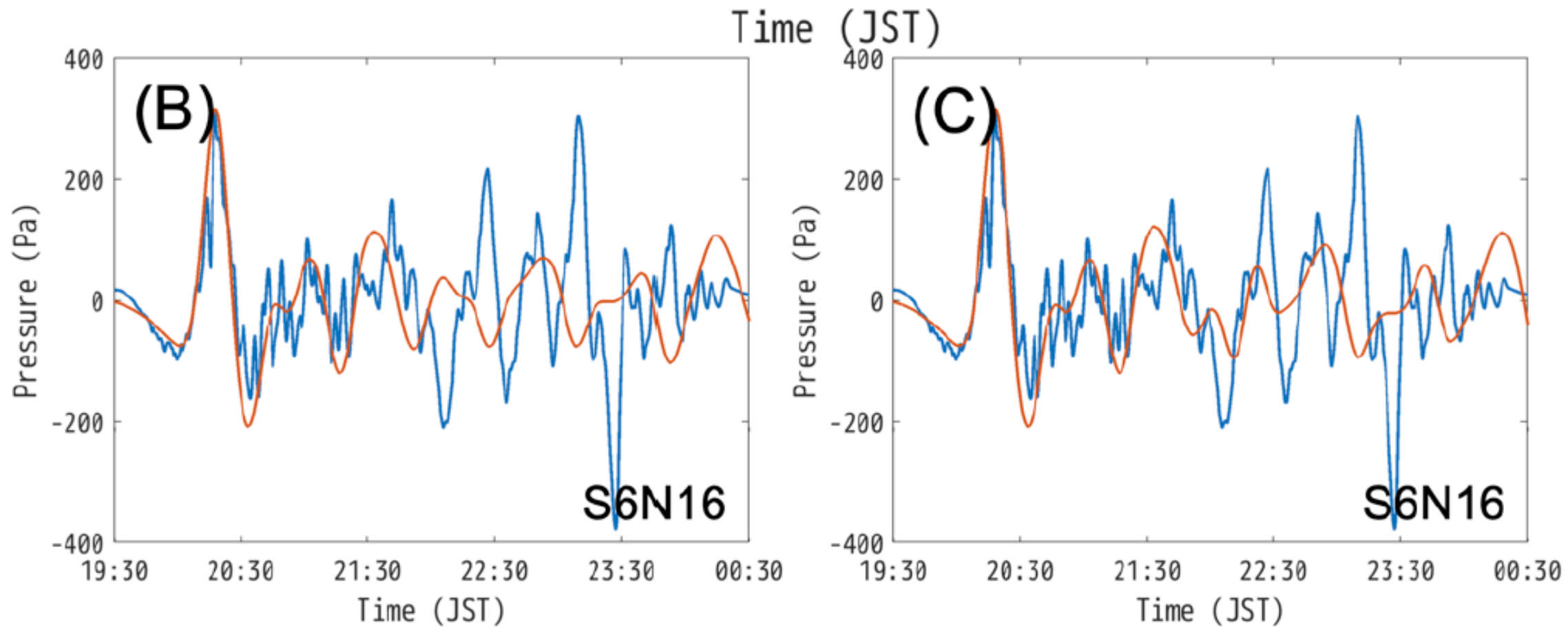
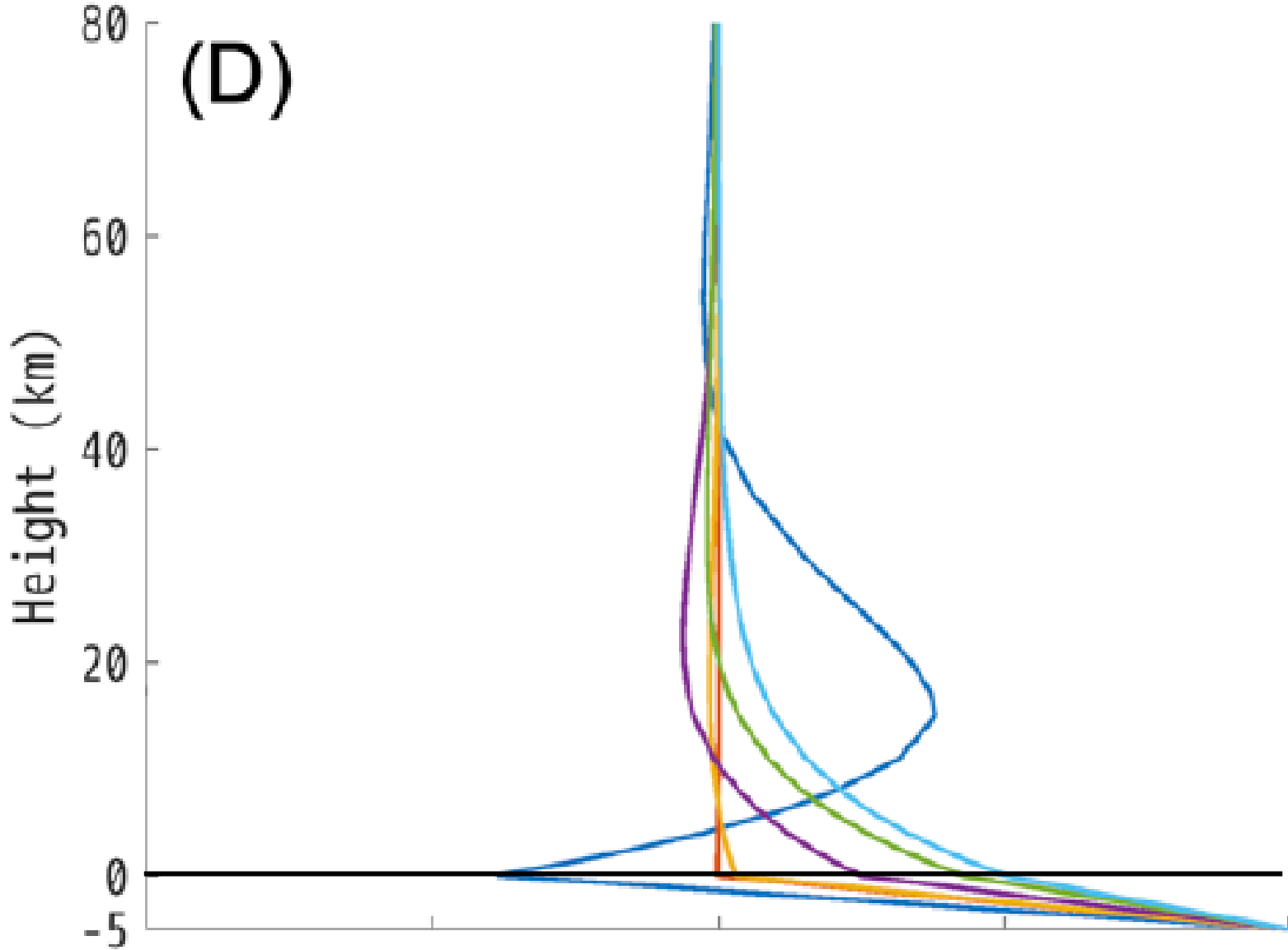


Figure 4.6: Observation (blue) and Synthetic (orange) records of (A) the barometer at Katahira station, and (B), (C) the OBP gauge at S6N16 station. The synthetic OBP record of (B) was calculated under the consideration only of the Lamb wave while (C) included both the Lamb and Pekeris waves. Note that all the observation waveforms were applied by a band-pass filter of 100–5000 s.

Period (s)

simulation)

(D)

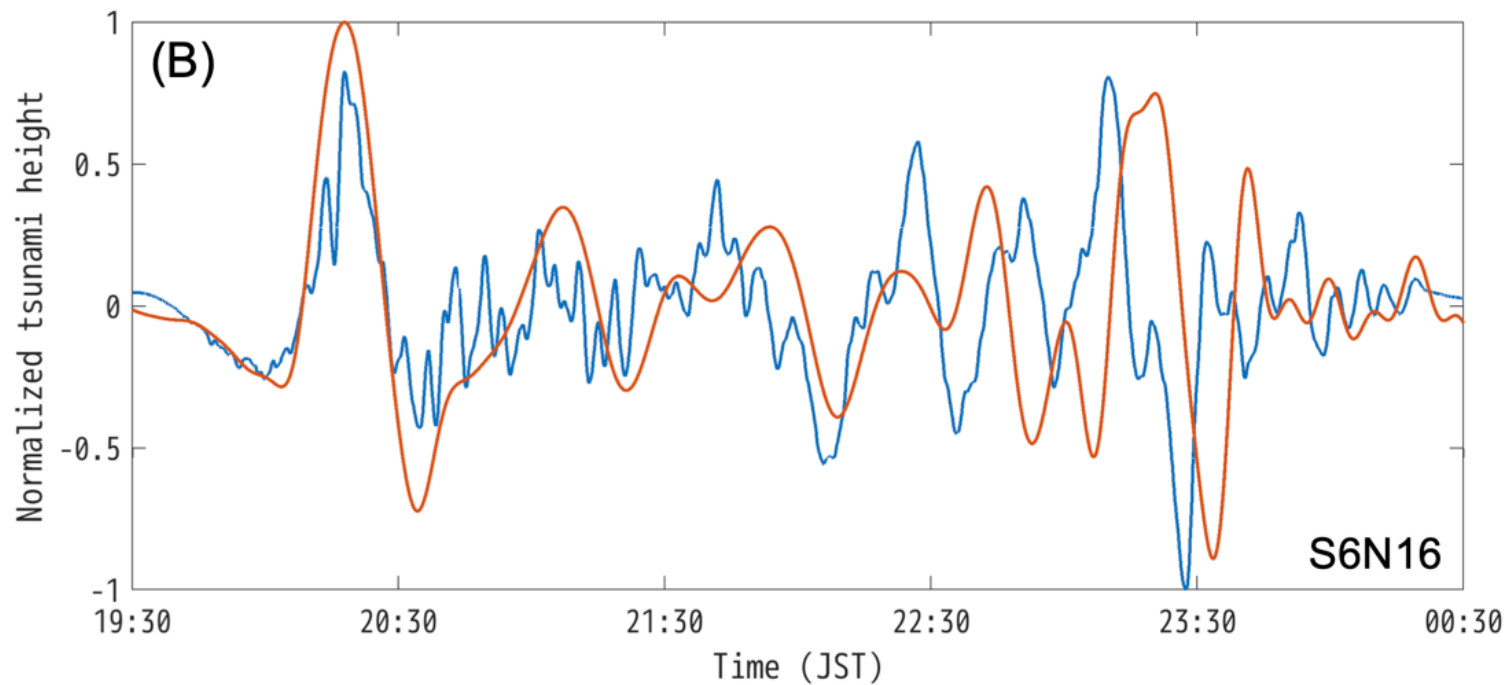
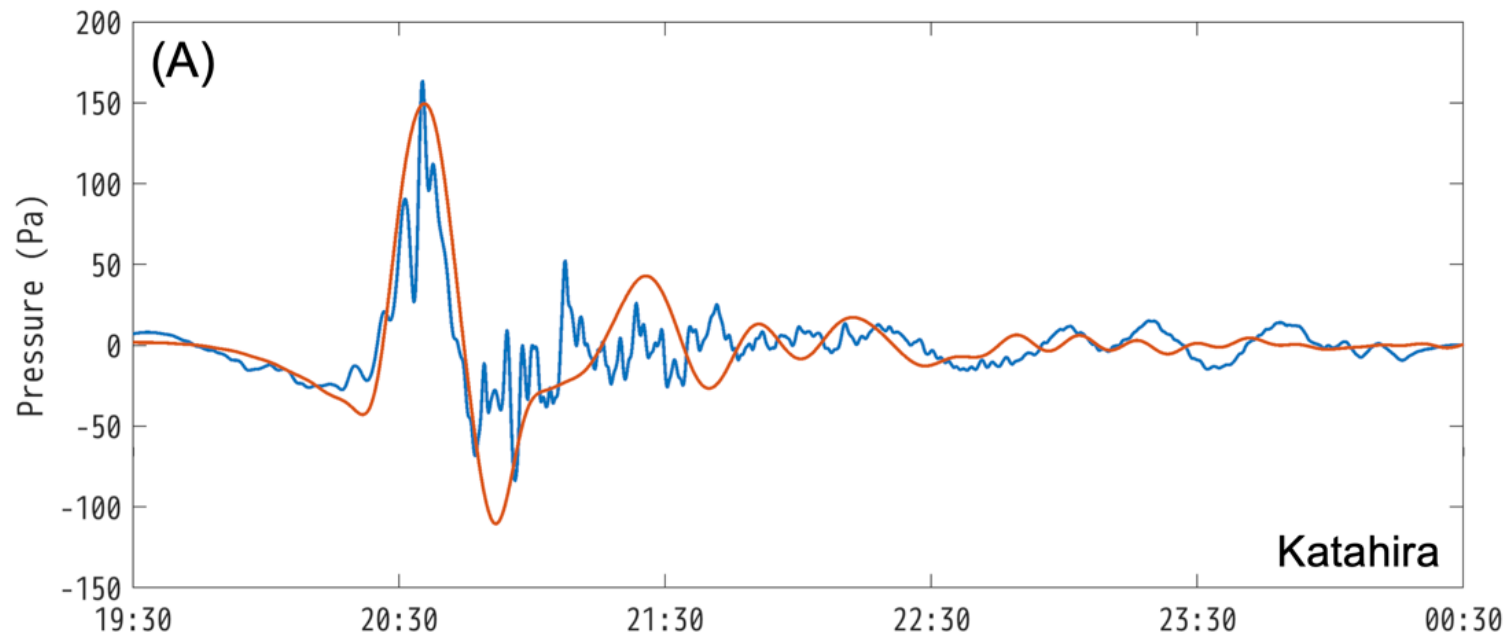


(A) Atmospheric sound speed model used in this study. The number of layers is 36. Note that upon the calculation of normal modes, an ocean layer was added to the bottom of this model.

(B) Phase and (C) group speed dispersion curves. The cyan, green, purple, yellow, orange, and blue lines represent GR0, GR1, GR2, GR3, GW0, and GR4 modes.

(D) Eigenfunctions of pressure for each mode at a period of 2000 sec. The colors are the same as (B).

The ocean layer is represented as a negative height (-5 km).



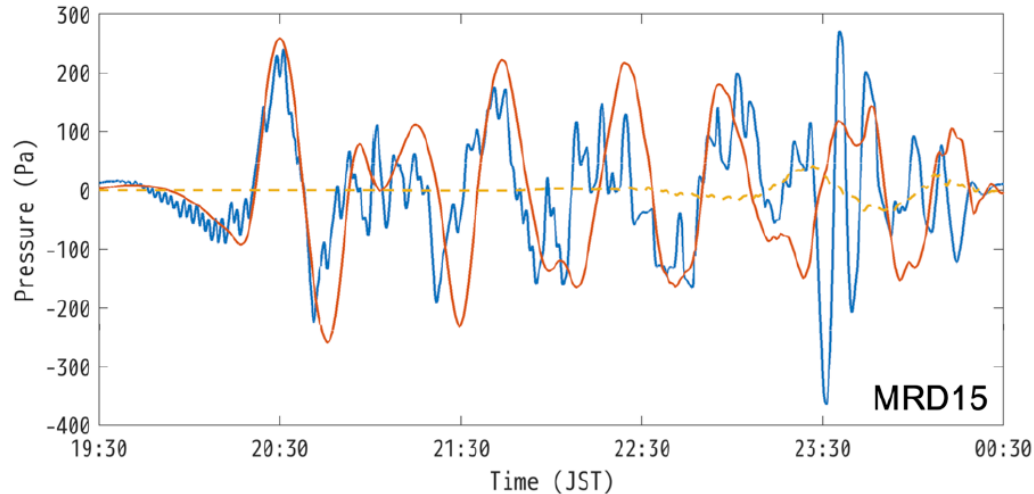
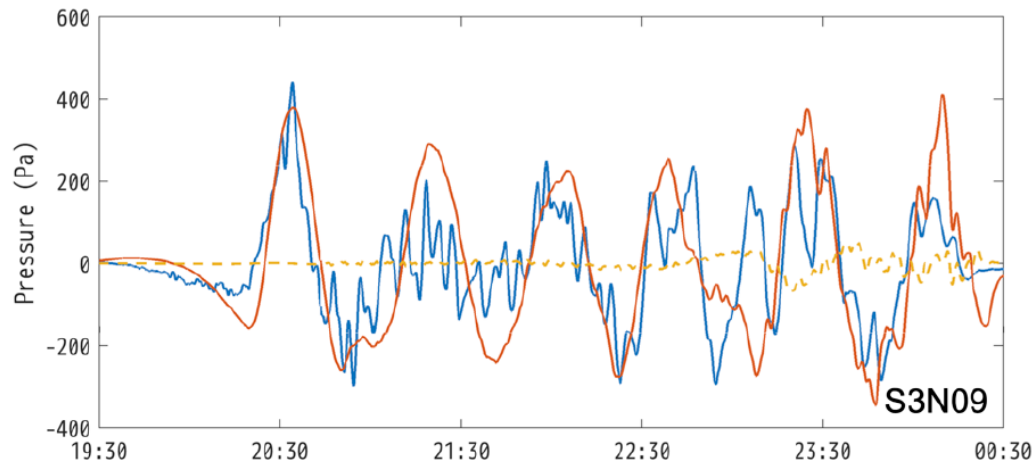
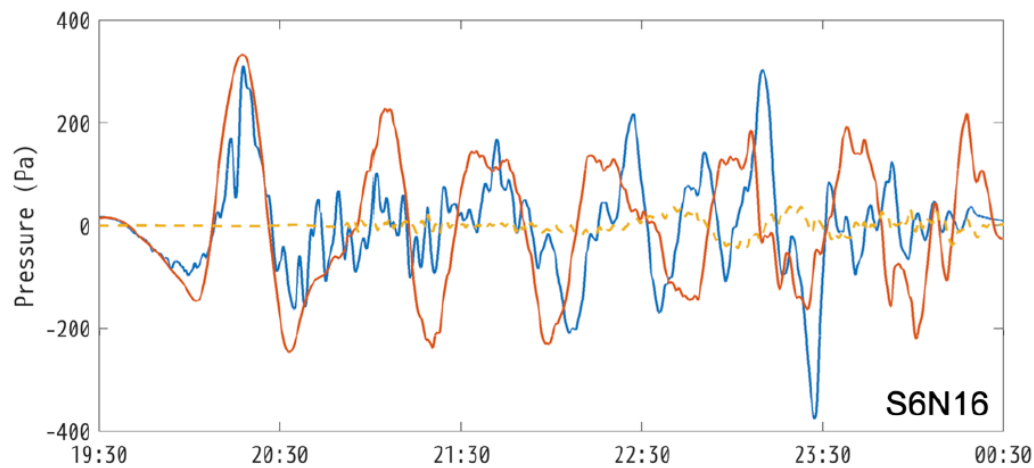
(A) Comparison of the synthetic (orange) and observed (blue) atmospheric pressure changes for the barogram at Katahira station.

(B) Normalized waveforms of the synthetic sea surface height (orange) and OBP gauge record (blue) at S6N16 station.

The maximum values are 1.4 cm and 3.8 cm, respectively.

Each synthetic wave is time-shifted so that the first arrival wave agrees with the observation.

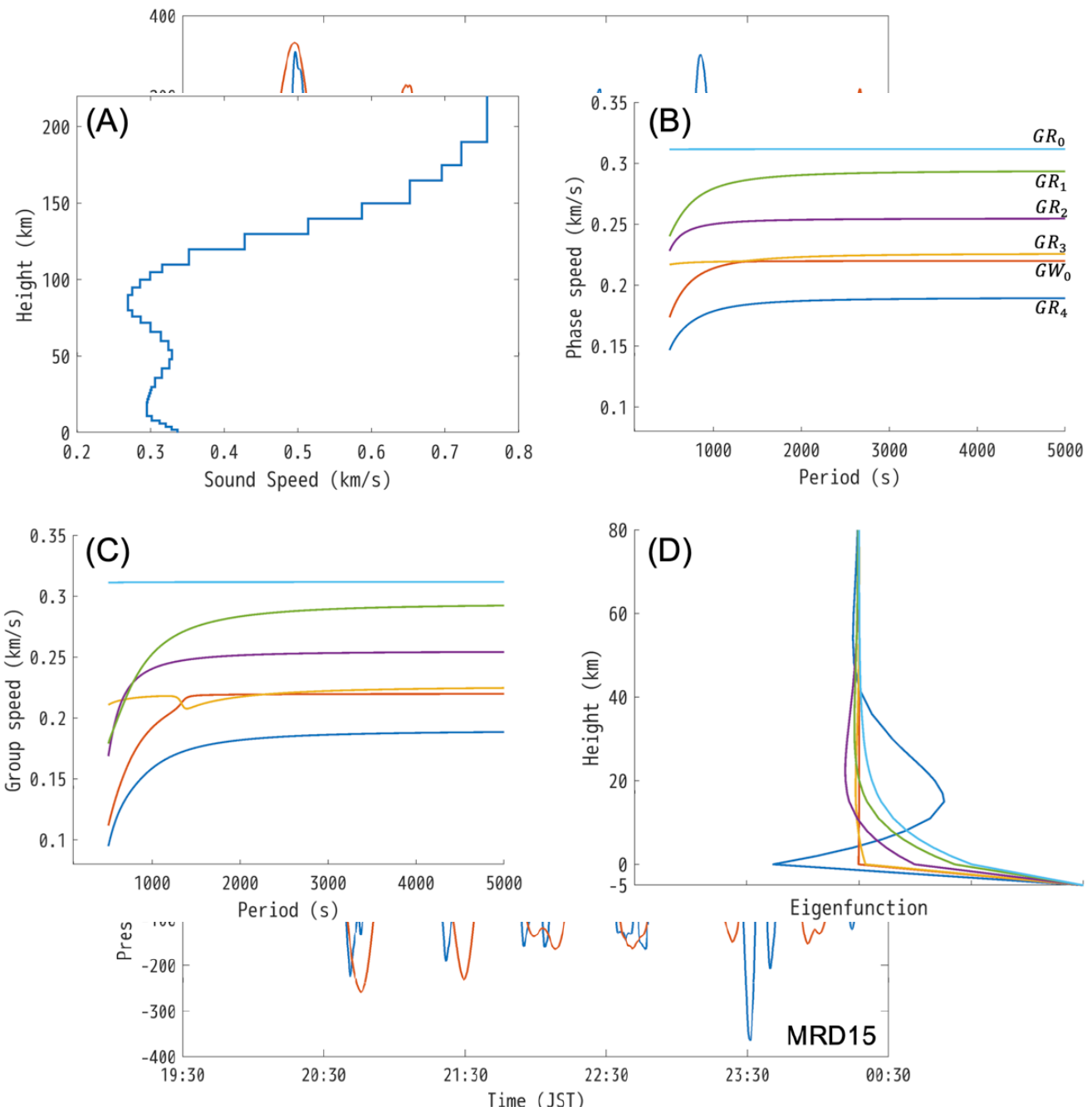
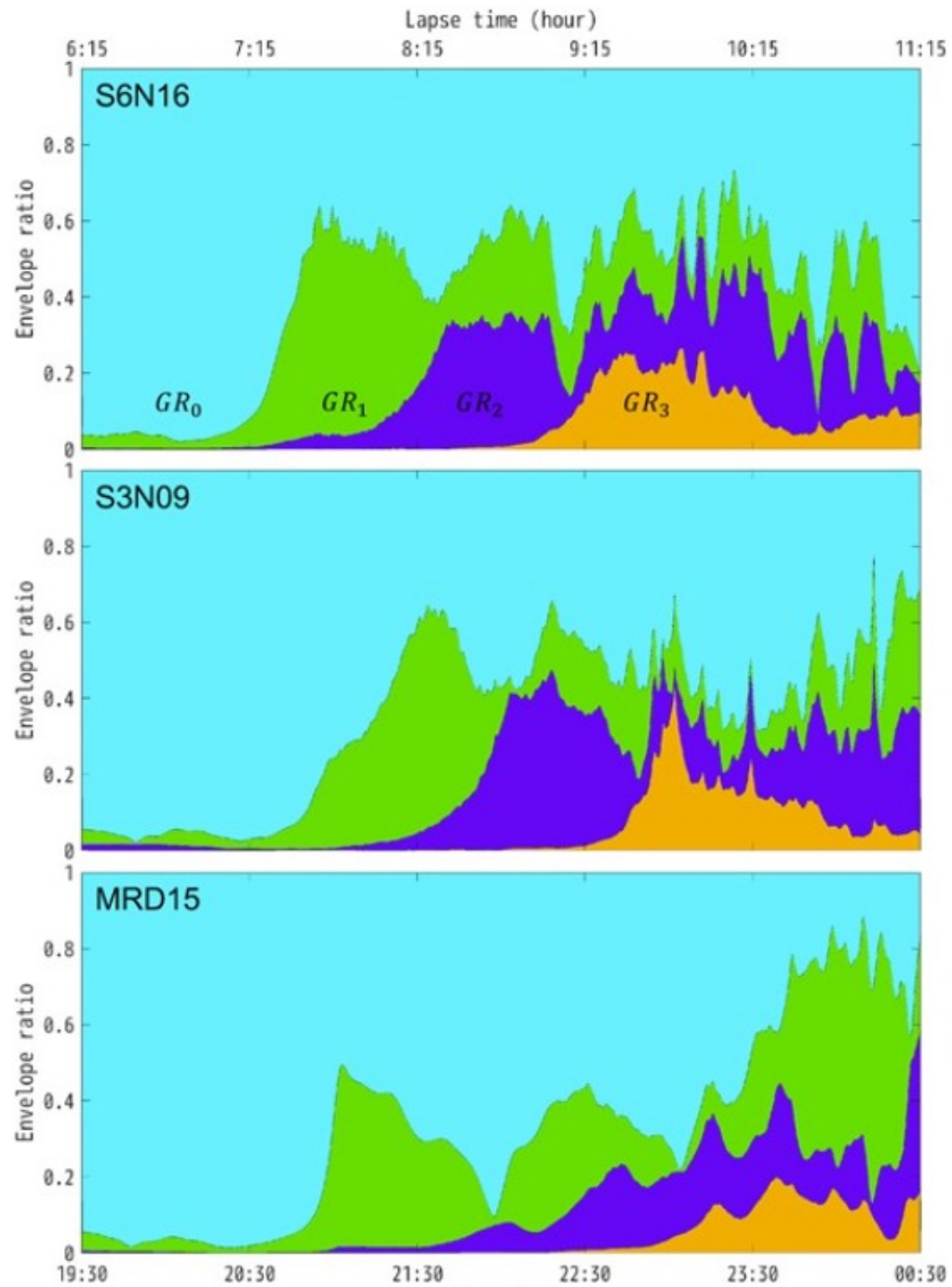
Note that the source-station distances are (A) 8000 km and (B) 7630 km to reflect the actual values, respectively.



Comparison of the OBP observation records (blue) and the synthetic waves (orange) by the hybrid calculation of the finite difference method and the normal mode theory at stations S6N16, S3N09, and MRD15.

The yellow dashed lines represent the GW_0 mode.

A band-pass filter of 100–5000 sec was applied to both the observed and synthetics. Note that the synthetic waves were time-shifted to agree with the first arrival of the observed ones.



Mechanisms of tsunami generations

Near field-tsunami

1. Underwater explosion
2. Lamb wave (Lamb wave + bathymetry effect (such as trench))
3. Pyroclastic flow
4. Flank Failure
5. Caldera subsidence
6. Lahar

Far-field-tsunami

Air-wave

Lamb wave (Lamb wave + bathymetry effect (such as trench))

(fundamental mode of atmospheric wave)

Higher modes of atmospheric wave